2016-01-01

Design Of A Thermal Management System For An Oxy-Methane Direct Power Extraction Combustor

Jad Gerges Aboud
University of Texas at El Paso, Jaboud@miners.utep.edu

DESIGN OF A THERMAL MANAGEMENT SYSTEM FOR AN OXY-METHANE DIRECT POWER EXTRACTION COMBUSTOR

JAD GERGES ABOUD

Master's Program in Mechanical Engineering

APPROVED:

Norman Love, Ph.D., Chair

Ahsan R. Choudhuri, Ph.D.

Tzu-Liang (Bill) Tseng, Ph.D.

Charles Ambler, Ph.D.
Dean of the Graduate School

DEDICATION

I dedicate this thesis to my parents and my aunt's family. I'm here because of your support and sacrifices Thanks also to Dr. Norman Love, for giving me the opportunity to acquire engineering experience that I will carry on for the rest of my life

DESIGN OF A THERMAL MANAGEMENT SYSTEM FOR AN OXY-METHANE DIRECT POWER EXTRACTION COMBUSTOR

by

JAD GERGES ABOUD,

THESIS

Presented to the Faculty of the Graduate School of

Department of Mechanical Engineering

The University of Texas at El Paso

in Partial Fulfillment

of the Requirements

for the Degree of

MASTER OF SCIENCE

DEPARTMENT OF MECHANICAL ENGINEERING

THE UNIVERSITY OF TEXAS AT EL PASO

December 2016

ACKNOWLEDGEMENTS

The research is supported by the US Department of Energy, under award DE-FE-0024062 (Project Manager Jason Hissam). However, any opinions, findings, conclusions, or recommendations expressed herein are those of the authors and do not necessarily reflect the views of the Department of Energy.

ABSTRACT

The overarching goal of this thesis is to present the design of a thermal management system for an oxy-methane direct power extraction combustor. The design is initiated by performing a 2D analysis on the combustor geometry and then using these results in a 3D model. This is done by using results for heat transfer coefficient and temperatures found from the 2D simulation and importing these to the 3D model. The approach used here couples the combustion process, heat transfer through the chamber wall, and fluid flow behaviors in order to observe the thermal characteristics of the combustor during operation. This approach is used as a design tool to build the combustor. After construction of the combustor, data from experimental tests were used to validate the simulation results. This experiment revealed that the data from the coupled simulations match the results of the experiments within 10%. Thus, this simulation may be used for the further experimental design of similar systems.

TABLE OF CONTENTS

LIST OF TABLES

LIST OF PLOTS

LIST OF FIGURES

1. CHAPTER 1: INTRODUCTION AND BACKGROUND

1.1. Overview

Electricity is the major source of energy that powers modern society. It lights buildings and streets, runs computers and telephones, drives trains and subways, and operates all variety of motors and machines. [1]. Since the electric power generation and distribution system has evolved; economics, technological advancements, and government regulations have been the main factors and motivation for development and production of power systems. These power systems are dependable and environmentally safe [2]. Many ways have been developed to produce electricity. Large power plants have been built to provide the large amounts of steady power demanded by modern societies. [1]

Different generating plants harness different energy sources to make electric power. The two most common types of generating plants are referred to in this thesis are Thermal Power Plants and Kinetic Power Plants. In Thermal Power Plants, the chemical energy in a fuel is first converted to heat then converted to generate electricity. As shown in section B of Figure 1, the heat from burning the fuel turns the water to high-temperature steam. Then this steam is directed through the turbine in section A. The steam pressure is converted to velocity which then spins the turbine blades. This shaft is connected to the rotor of a generator that produces electricity, section C in Fig. 1.

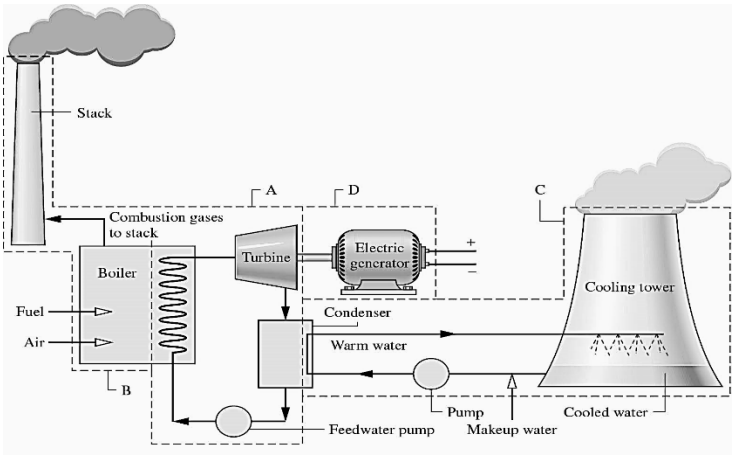

Figure 1 Thermal power plant schematic

On the other hand, in Kinetic Power Plants potential energy is converted to kinetic energy which is converted into electricity. A moving working fluid, such as water, spin a turbine. The turbine motion spins the rotor of a generator to produce electricity. As shown in Figure 2, water from a reservoir behind the dam in section A is channeled to the turbine in section C through penstock in section B. After flow exchanging momentum with turbine blades causing the shaft to spin. This shaft is connected to the rotor of a generator that produces electricity in section D.

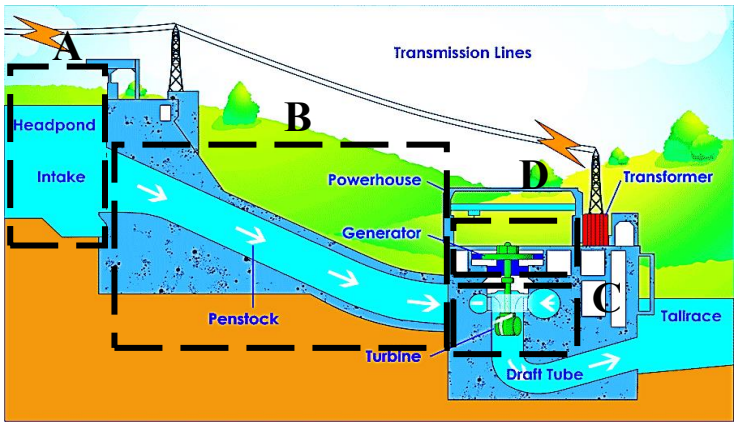

Figure 2 Kinetic power plants schematic

1.2.Negative Aspects of Traditional Power Sources

In most large stationary Power Plants power is generated using fossil fuels. [1] The main emissions of burning fossil fuels with air are the greenhouse gasses such as carbon dioxide, methane, nitrous oxide, and fluorinated gasses. For instance, fossil fuels used to generate electricity were responsible for 30% of the 6,870 million metric tons of greenhouse gas emitted in the United States in 2014 [3]. Carbon dioxide makes up 81% of the total greenhouse gas emissions while methane, nitrous oxide, and fluorinated gasses from 11%, 6%, and 3% respectively as it shown in Figure 3.

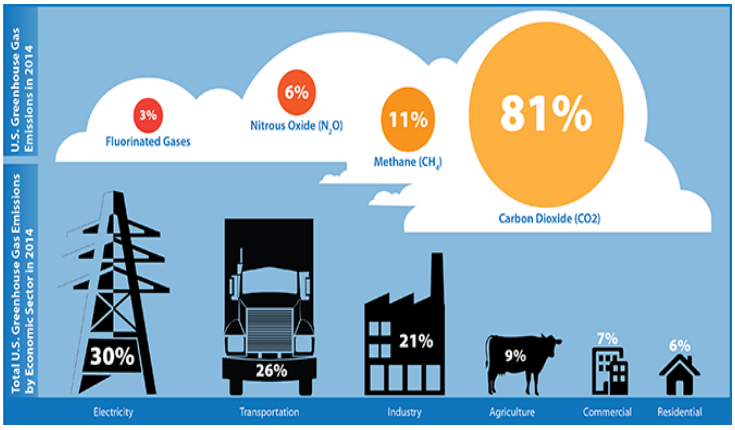

Figure 3 U.S. Greenhouse Gas emissions in 2014

Although carbon dioxide is the primary pollutant of greenhouse gasses, power plant also emits other contaminants as well. For example, power generation contributes about 70% of total sulfur oxides including SO_2, 20% of overall NOx, and 40% of mercury emissions. These emissions do not only cause health issues to humans but also impact the environment.

One important parameter to consider for emissions is the residence time, which is the amount of time it takes for a combustion particle to reach a certain boundary. This time may differ from few days to several years. When the pollutants fall back to the ground they react with atmosphere element such as rain, snow, fog, gasses causing harm to the environment. From SO_2 and NOx interactions with atmosphere elements, acidic mixtures, small particles, and ozone are formed.

Lakes and rivers become more acidic from the dissolved pollutants . Smog which forms from small particles shaped by SO_2 and NOx reduce visibility and may cause severe respiratory problems in humans' daily activities. Mercury is deposited in water bodies and is consumed by fish, fish-eating birds and mammals. Humans then can consume these contaminated animals and after a prolonged exposure suffers neurological damage. [4].

Wastewater from a power plant can carry pollutants into watersheds. Kinetic Power Plants require complex technologies and infrastructures which are difficult to build and maintain. Technical problems such as continuously operating and efficiency are also concerns for this type of plant. Other types of power plants replace some of the traditional equipment with natural sources to produce electricity. Geothermal plants, for example, replace boilers with the heat from the Earth. Photovoltaic materials and fuel cells go further by dispensing with turbogenerators entirely. Although fossil-fuel plants can create serious environmental problems, they are still used in the U.S. today. Even with strict pollution controls, waste material is still produced. Carbon dioxide gas and ash are the current concerns from coal-based plants for example. [1].

Efforts have been undertaken to develop and improve renewable and alternative sources such as solar, the wind, tide, and Geothermal. Use of these other power sources has increased in the last 30 years in an attempt to replace fossil fuels. For example, in United states the consumption of renewable energy in 2010 rose by 6% [5]. In 2015, the renewable share of energy consumption in the United States was nearly 10%. The greatest growth in renewables over the past decade has been in solar and wind electricity generation. Also, the use of liquid biofuels has improved in recent years. [6]. Nonetheless, this growth has been very slow and will require extensive time and new technologies to be effective as existing power plants in the future. Therefore, developing advanced technologies that increase the power generation efficiency for new plants and technologies to capture carbon dioxide from industrial and power plants are necessary.

Gas turbines have been an incredible source of reliability, efficiency, and have been developed and improved to operate at high temperatures using air-combustion-approximately 1800 K. However, this temperature limit exceeded when considering oxy-combustion. The advantage of an oxy-combustion system is that the products are carbon dioxide and H_2O. From the products H2O, can be condensed and the carbon dioxide sequestered. However, the flame temperature for an oxy-combustion system can exceed 3000 K, which is well above current operability limits of the combustor and gas turbine systems in use. To reduce flame temperatures, fuel is typically mixed with recycled carbon dioxide or other diluents which result in overall lower system efficiency. One system capable of efficiently utilizing this energy with carbon capture is Magnetohydrodynamic (MHD) generators which are a type of direct power extraction, which transfer the thermal to electrical energy directly without using the mechanical energy. Therefore, using Magnetohydrodynamic technology to generate power is a possible solution that efficiently produces electricity with low emissions.

1.3.Fundamental Concept of a Generator

Most power plants make electricity with a machine called a generator which has two important parts: the rotor and the stator. Generators use electromagnetic induction principle, which uses the relation between magnetism and electricity. While magnets rotate around a stationary stator, the magnets induce an electric current in the wire. Both thermal and Kinetic plants use the turbine to spin the generator to generate the electricity. These generators use Faraday's principle and Lorentz Force to transfer the mechanical energy to electrical energy. In early 19th century, Michael Faraday developed the fundamental concept and formed the basis for the electrical power generation. [7]. During his first studies, he established Faraday's law of induction. In this, he described how the electric circuits and magnetic fields would interact to create an electromotive force. This phenomenon is called electromagnetic induction [8]. In theory, the solid conductor could be replaced by ionized gasses and electromagnetic induction will occur and electricity will be generated. This behavior of conducting ionized gasses -or plasma- in the magnetic field called Magnetohydrodynamic (MHD). [9] Faraday discovered the basic MHD effects using the water flow in a river in 1832. Maxwell then formulated this concept through mathematical equations, leading to the theory of thermal ionization in 1920. But an MHD system was not achievable until1940 when Karlovitz and Halasz

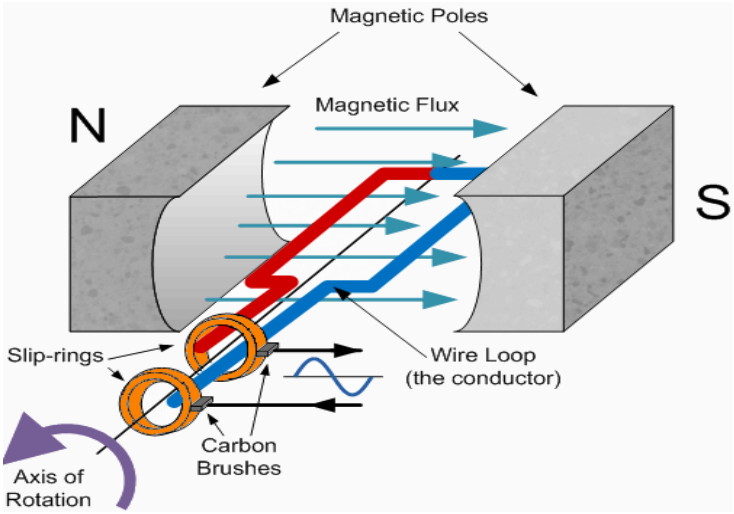

Figure 4 schematic of simple generator

received the patent for the first MHD system. Since the first patent in the late 20th century an enormous effort was directed to develop, test and improve MHD generators [7]

1.4.History of Magnetohydrodynamics

Since 1970, several countries such as Russia, Japan, China and the United States have undertaken MHD research programs with a particular emphasis on the use of coal as a fuel. [7]. The reason behind that was the capability of MHD power generator to convert the enthalpy from a high temperature working fluid into electrical power [10]. The simplicity of the system is preferred in the industry due to the fact that MHD generators have no mechanically moving parts. Therefore, the electrical energy is directly converted from thermal energy [11].

Based on the type of heating method used for the working gasses, MHD generators are categorized into open-cycle and closed-cycle. For open-cycle systems, the working fluids are the products of a fossil fuel combustion plasma such as carbon dioxide and water [11] [12]. Closed-cycle systems usually use a noble gas non-equilibrium plasma. [13]. For both open-cycle and closed-cycle MHD generators, it is common to seed the fluid with an alkali metal such as potassium or cesium. Cesium, which has an ionization potential of 3.89 eV, would be the ideal seed material for MHD generators but the cost of Cesium makes it not profitable. Potassium, which has an ionization potential of 4.34 eV, is the typical choice for the seed in the MHD generators. To achieve the required electrical conductivity, the gas is seeded with a material of low ionization potential. Seed fractions of the order of 0.1% to 1% are representative of noble-gas and combustion MHD plasmas, respectively [14].Unseeded fluids may also be used in MHD systems through two methods: high voltage pulsars, which are used to ionize the gasses only for the time that its fluid will be passing through the MHD channel and by high-temperature plasma, which has also been used to ionize the working medium. [15]

The electrical conductivity of the working medium has a major role in MHD devices. Electrical conductivity is a function of gas temperature, the density of charged carriers and electron mobility [16]. Previous studies have shown that electrical conductivity of gasses is effectively zero at temperatures below 2300 K [11]. Therefore, the main requirement is maintaining the combustion temperatures at the exit of the nozzle above 2300 K to sufficiently provide electrical conductivity in the gas and to deliver a uniform ionized gas velocity through a magnetic field.

MHD generators are complex systems composed of different parts: combustor, converging-diverging nozzles, and a magnetic field. [16]The first part of the system is the combustor which includes fuel injector, igniter and combustion chamber. After the gasses combust high temperature ionized the products , the products are directed through the converging-diverging nozzle that accelerates gasses to supersonic velocity. After the nozzle, the hot gasses travel through an electromagnetic field where the power is generated. Following Fleming's Right Hand Rule, as the gaseous conductor moves through the magnetic field it generates an electrical current perpendicular to the magnetic field and the conductor's direction of flow [11].

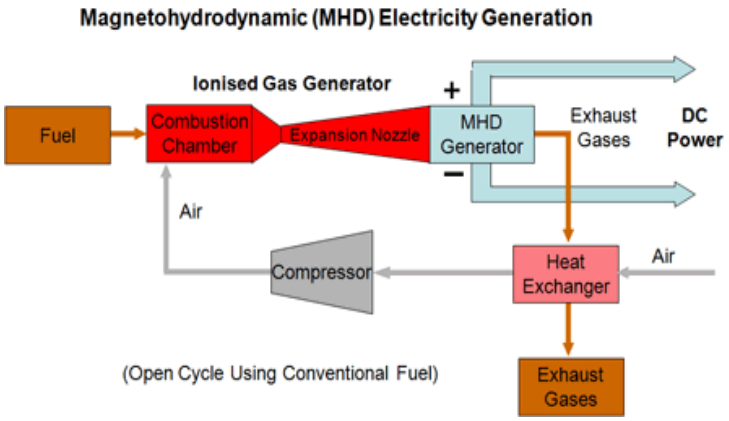

Figure 5 schematic of Open cycle MHD power generator

In general, higher velocities at the entry point of the magnetic field are preferred since higher velocity generate higher currents according to Faraday's Law of induction. Also, higher velocity comes with higher Mach numbers range from 1 to 5 [11], [15], [17]. In order to achieve such high velocity, high pressure with a strong combustion event associated with the converging-

diverging nozzle is needed. Which in turn leads to higher temperatures ranging from 1500 to 3100 K [12], [18], [11], [13]. Lastly, the magnetic induction produced by the magnetic field ranges from 2 to 6 Tesla [11], [13], [17]. This high velocity, high temperature, and high magnetic field are used in several attempts at MHD power generation such as the Sakhalin, AVCO, Mark VI, and etc. For example, the generator achieved velocities of 2050 m/s, a Mach number of 2.4, temperatures as high as 2750 K, and a maximum magnet induction of 2.5 T at the inlet of the electrode section in Pulsed large-scale open-cycle MHD generator with a Faraday MHD channel as it used in Sakhalin, [13]. Also, the Mark II generator, which used segmented Faraday MHD channels showed lower velocities by contrast at only 887 m/s but it did show temperatures of 2971 K and a maximum magnetic field of 2.12 T [18].

The magnet field and electrodes are coupled at the nozzle attachment. Electrodes are the place where the current is generated from the magnet field for the MHD systems according to Faraday's Law of induction. However, since configurations for MHD generators tend to vary, this leads to different types of electrodes being used. There are 4 main types of electrodes: Faraday, Hall, diagonal, and disk as shown in Figure 6. [14] A finite segmented Faraday generator fundamentally differs in electrical connection from the diagonally connected generators and the Hall connected generators, and each separated electrode is individually

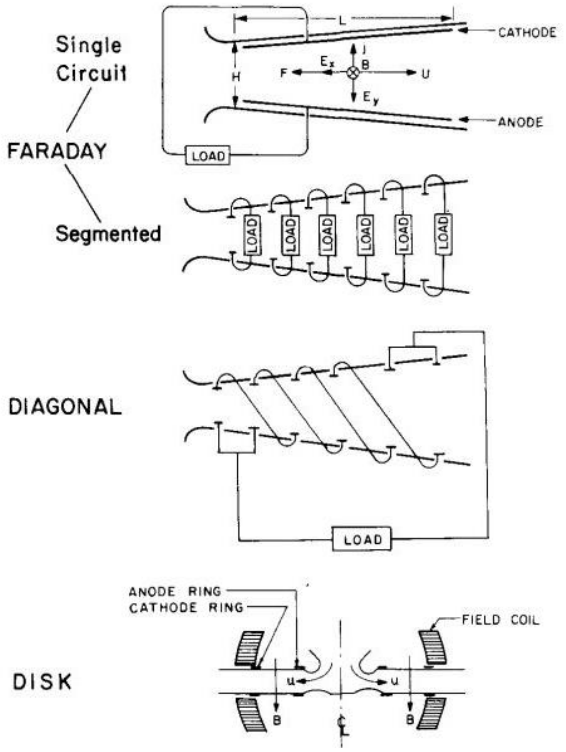

Figure 6 MHD Generator Configurations [14]

connected to an external load. [19]The disk-type channel consists of two insulator disks with inner and outer ring electrodes [11]. Testing has found that the Faraday electrodes are best in a wide range of areas including efficiency, voltage drop, and maximum power output. However, increases the complexity of these types of electrodes, increases maintenance and cost; for this reason, the diagonal electrodes are preferred. [19]

MHD power generation systems' efficiency is usually described in terms of enthalpy extraction ratio, which is the ratio of power output over thermal input [20]. Extraction ratios can range from 10 – 30% [11], [20]. Open-cycle generators, as recently as 2004, have experimentally demonstrated a 15% enthalpy extraction ratio for a shock-driven disk channel and 11% for a linear Faraday channel which had a 3.2 T of the magnetic field. This last come from the Arnold Engineering Development Center (AEDC) in Tullahoma, Tennessee, using 300 MW of heat input [20] Sakhalin also showed enthalpy extraction ratios at this range at 12 % [17] These low efficiencies are potentially due to the lack of research in this area. More experimental research into MHD generators may produce higher enthalpy extraction ratios.

As stated previously, products temperatures in the MHD system range from 1500 to 3100 K. In order to keep the temperatures of the combustion chamber and Nozzle walls within their allowed limits, the significant cooling effort is needed [21]. Due to the nature of the problem, an accurate solution must effectively couple combustion gas properties, high-temperature material characteristics, and coolant flow. Many works have been done with a cooling system with analytical and numerical approaches. These approaches vary from the use of 1-D semi-empirical correlations to computationally expensive three-dimensional approaches. Marchi et al [22] presented a one-dimensional mathematical model using three coupled subproblems in including the combustion/wall/coolant configuration. This approach seems to diverge from the majority, as

most groups have attempted to characterize nozzle heat transfer through 2-D or 3-D computational solutions. While, Kim et al [23], [24] employed a combination of numerical methods with semi-empirical correlations to be used in an actual regeneratively cooled thrust chamber and validated against the measurement of hot-firing tests in terms of temperature increase and pressure drop of the coolant through the cooling passages. Likewise, Zhang et al [25] modeled combustion gas employing a two-dimensional axisymmetric simulation. In addition, Pizzarelli et al [26] [27] have presented various works based on this methodology. Wang et al [28] compared heat fluxes to published data from the SSME's combustion chamber. This investigation employed a 3-D heat conduction sub-model and a 1-D channel hydraulic model. Their iterative procedure was quoted to compute heat flux results that were very similar to experimental data.

These studies found that the use of a simple resistance model was effective in characterizing temperature and pressure drop distributions in cooling channels. Obstacles and geometric irregularities in the coolant flow can result in increased pressure drop and localized hot-spots. One of such investigations [29] focused on the optimization of fuel injection ports for use in scramjet cooling systems. By employing a circular model as a baseline, this group optimized obstruction geometries through the addition of a smooth transition structure and widening of channels around the critical area.

1.5. Project impact

As stated before, much work has been done but there are still many unanswered questions regarding open-cycle MHD generation systems and especially the cooling system. Under steady-state operation for MHD generator, the heat fluxes are expected to be about 7 MW/m^2 as Vidana et al [30] and Hernandez et al [16] stated. This significate heat flux is due to supersonic nozzle characteristics with oxy-methane combustion. Also, this heat flux is the main requirement to ionize

the product to generate electricity; at the same time, it generates very high temperature- about 3000 K in the gaseous side. After this temperature transferred to the wall of the combustor, the temperature will be above the melting point of most material alloys. In addition, the material strength drops dramatically at high temperatures. The MHD system is a complex system, and it involves high-temperature combustion products. This temperature is required to ionized the gasses to generate electrical power. on the other hand, this high gas temperature raises the combustor wall temperature requiring a significant cooling system.

1.6.Objective

The analysis of the flow behavior and the heat transfer characteristics in a regeneratively cooled combustion chamber is of paramount importance for the development of a high-performance, steady-state Oxy-Methane combustion for the power generator. and to ensure the combustor structural will not fail due to thermal effect. The exact analysis of such a problem is difficult and can only be obtained by experiments or by complex numerical simulations of the coolant flow and wall heat transfer.

This thesis will present the design of a thermal management system for an Oxy-Methane combustor. Current design constraints dictate that the cooling system must be operational for an indefinite period of time. For this reason, the channel design deviates from the typical regenerative cooling approach, where the coolant is injected into the chamber.

A coupled analysis is performed by modeling a 2D case with the hot-gas/wall/ coolant and export these properties to a 3D model of wall/ coolant using Reynolds-Averaged Naiver-Stokes (RANS) equations. After that, the results from the 3D model will be compared with numerical results and experimental data.

The current design constraints dictate that the cooling system must be operational for an indefinite period of time. For this reason, the channel design deviates from the typical regenerative cooling approach, where the coolant is injected into the chamber.

1.7. Organization of thesis

- In chapter one, a background and fundamental Concept of power generators will be presented. Also, a literature review on MHD and the main objective of the thesis.
- In chapter two, the main approach of heat transfer will be developed. In addition, the methodology of design, computational and experimental were specified.
- In chapter three, the computational model properties such as mesh and boundary condition will be specified and the experimental cases were presented.
- In chapter four, a comparison between the design, computational model and experimental cases will be discussed.
- In chapter five, is the summary of the thesis

2. CHAPTER 2 METHODOLOGY

2.1.General approach

As it stated in chapter 1, a computational model for the cooling system has two parts, 2D, and 3D models. In the 2D model, a fully-coupled axisymmetric model combining three domains combustion, wall, and cooling. was developed and integrated into ANSYS FLUENT. The three domains are used in one simulation to estimate the heat flux and temperature at the combustion properties. In the 3D model, the heat flux from the 2D model is imported as a boundary condition at the combustion wall as well. The results acquired from the 3D model will be compared with experimental results obtain from an Oxy-Methane Combustor.

2.2.Experimental Methodology

2.2.1. TEST ARTICLE

As it shown in Figure 7 the Direct Power Extraction Combustor made up of different parts. Combustion chamber, nozzle, and barrel that have been manufactured from a single rod of superalloy Inconel 718. As it shown in Figure 7 the cooling channels are very difficult to be manufactured in the traditional way such as milling or lathing. Therefore, cooling channels were made through the electrical discharge machining method (EDM). The process consists of removing

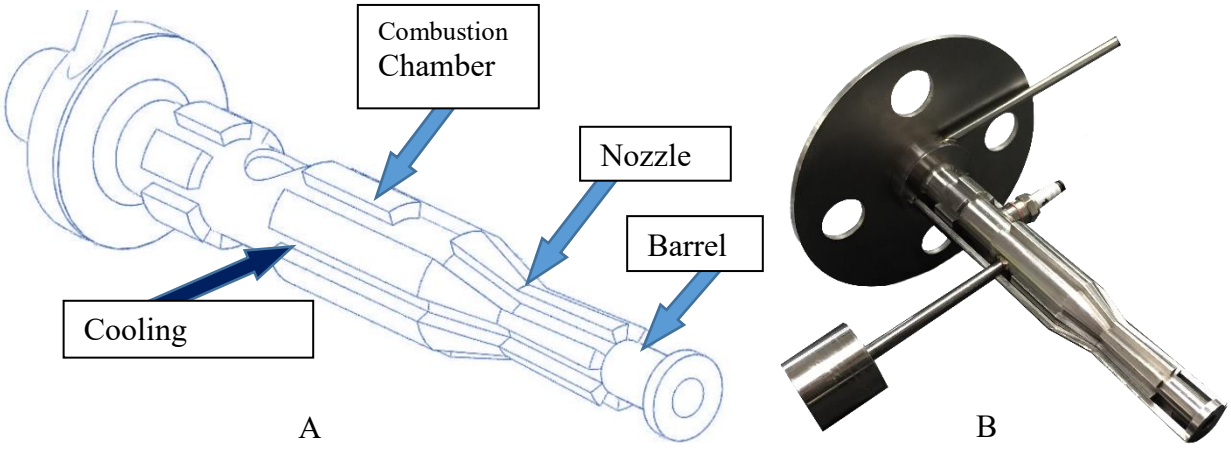

Figure 7 Internal Drawing of Oxy-Methane Direct Power Extraction

material from the workpiece using electrical discharges. In order to enhance the cooling

capabilities, the DPE combustor contains six channels to increase convective and conductive heat transferred rate. They are designed to direct and increase the velocity of the coolant.

Two symmetrical closeouts, injector attachment, and all additional connections, as it shown in Figure 8-A, have been laser welded with to fabricated combustor to ensure accuracy, prevent leaking and create coolant path. Two sensor and instrument ports have been added to the channel structure, these ports cause the flow obstruction. The flow obstructions correspond to a surface thermocouple port, a pressure tap- that is orthogonal to the flows, and combustion ignition tube. The final result after manufacturing is shown in Figure 8-B.

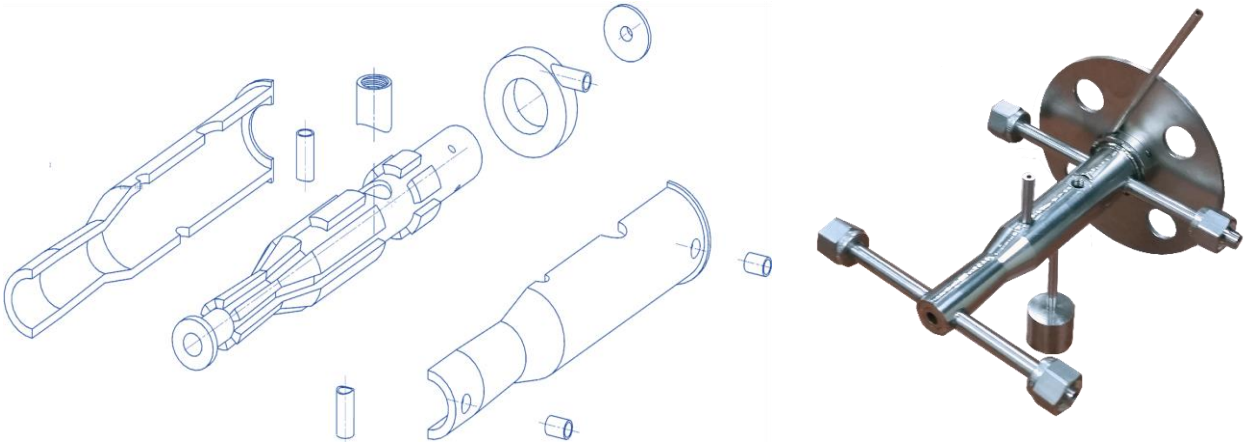

A **B**

Figure 8 Oxy-Methane Direct Power Extraction Combustor

Water was selected as the coolant due to its low viscosity and heat capacity. Nevertheless, due to its relatively low boiling temperature, the water must be introduced pressurized to increase its saturation temperature. The calculated required flow rate to effectively cool down the walls of the oxy-fuel combustor was approximately 16 LPM, for which a high-head, low-flow pump was selected. The water flows in a counter flow configuration entering near the exit of the nozzle and exits near the injector.

2.2.2. COOLING SYSTEMS

The schematic diagram for coolant and propellant feed system is outlined in Figure 9. The coolant delivery system included temperature, pressure and flow rate sensors. The flow meter measures the water volumetric flow rate in the system. The temperature sensors are placed at the entrance and exit of the test article to measure the water temperature during testing sessions. The pressure sensors measure the pressure variation within line component.

2.2.3. PROPELLANT FEED SYSTEM

Similarly, to the cooling system, the fuel and oxidizer lines are equipped with pressure, temperature and flow meter sensors. The pressure transducers are placed before entering the fuel injector and oxidizer port to provide an accurate reading for pressure drop in feed propellant manifold system. Also, the propellant manifold system incorporates mass flow meters to monitor flow variations during test sessions.

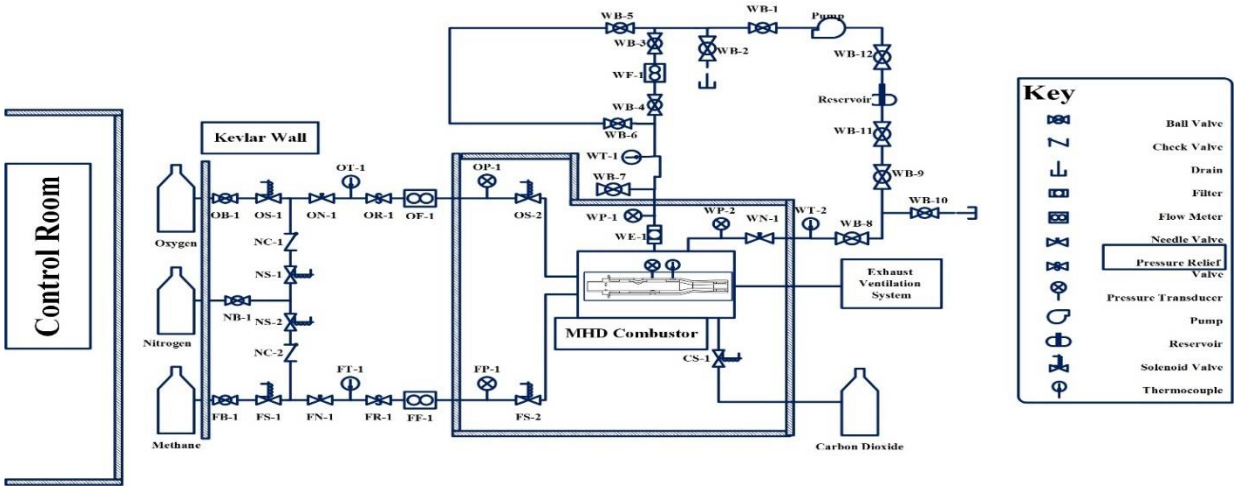

Figure 9 Propellant and cooling system for Oxy-Methane Direct Power Extraction Combustor

2.3.Numerical Methodology

CEA is a program which calculates chemical equilibrium product concentrations from any set of reactants and determines thermodynamic and transport properties of the product mixture. Built-in applications include calculation of theoretical rocket performance, shock tube parameters, and combustion properties. Therefore, this code is used to estimate the products properties', temperature and heat flux with isentropic flow relations.

A numerical method is used to estimate the cooling characteristic. The numerical problem required modeling steady-state, compressible and turbulent fluid flow with non-premix combustion. Therefore, ANSYS Fluent software package was used to solve this problem. ANSYS Fluent uses a range of mathematical models for transport phenomena -like heat transfer and chemical reactions. These mathematical models are combined with the complex geometries. The mathematical models solve conservation equations for mass, momentum, energy and species for the mixture fraction and its variance.

2.3.1. MASS AND MOMENTUM EQUATIONS

Reynolds-Averaged Navier-Stokes (RANS) equations are used to solve continuity and momentum Equations by taking a time average and they can be written in Cartesian tensor form as [31]

$$\frac{\partial \rho}{\partial t} + \frac{\partial}{\partial x_i}(\rho u_i) = 0 \tag{1}$$

$$\frac{\partial}{\partial t}(\rho u_i) + \frac{\partial}{\partial x_i}(\rho u_i u_j) = -\frac{\partial p}{\partial x_i} + \frac{\partial}{\partial x_i}\left[\mu\left(\frac{\partial u_i}{\partial x_j} + \frac{\partial u_j}{\partial x_i} - \frac{2}{3}\delta_{ij}\frac{\partial u_I}{\partial x_I}\right)\right] + \frac{\partial}{\partial x_j}\left(-\rho\overline{\acute{u}_i\acute{u}_j}\right) \tag{2}$$

Table 1 Mass and Momentum Governing Equation Variables

Symbol	Name
ρ	Density
t	Time
$x_i\ , x_j, x_I$	Position on i, j, I
u_i, u_j	Velocity on i, j
u_i', u_j'	Acceleration on i, j
δ_{ij}	

2.3.2. $k-\varepsilon$ EQUATIONS

The standard $k-\varepsilon$ model in ANSYS Fluent falls within turbulent model and has become the workhorse of practical engineering flow calculations and accuracy for a wide range of turbulent. Therefore, it will be the perfect model to be used in DPE Combustor. Theses equations are presented in Eqs. (3-5) [31]

$$\frac{\partial}{\partial t}(\rho k) + \frac{\partial}{\partial x_i}(\rho k u_i) = \frac{\partial}{\partial x_j}\left[\left(\mu + \frac{\mu_t}{\sigma_k}\right)\frac{\partial k}{\partial x_j}\right] + G_k + G_b - \rho\varepsilon - Y_M + S_k \tag{3}$$

$$\frac{\partial}{\partial t}(\rho \varepsilon) + \frac{\partial}{\partial x_i}(\rho \varepsilon u_i) = \frac{\partial}{\partial x_j}\left[\left(\mu + \frac{\mu_t}{\sigma_\varepsilon}\right)\frac{\partial \varepsilon}{\partial x_j}\right] + C_{1\epsilon}\frac{\varepsilon}{k}(G_k + C_{3\varepsilon}G_b) - C_{2\varepsilon}\rho\frac{\varepsilon^2}{k} - S_\varepsilon \tag{4}$$

The turbulent viscosity μ_t , is computed by combining k and ε as follows:

$$\mu_t = \rho C_\mu \frac{k^2}{\varepsilon} \tag{5}$$

Table 2 k-ε Governing Equation Variables

Symbol	Name
k	Turbulent kinetic energy
u_i	Velocity
Y_M	Overall dissipation rate
ε	Dissipation rate
c_p	Specific Heat
μ	Dynamic Viscosity
μ_t	Turbulent Viscosity
$\sigma_k, \sigma_\varepsilon$	Turbulent Prandtl Numbers for k, ε
G_b, G_k	Kinetic energy generation due to buoyancy, velocity
S_k , S_ε	User-Defined Source Terms
$C_{1\varepsilon}$, $C_{2\varepsilon}$, $C_{3\varepsilon}$, C_μ	Constant

2.3.3. NON-PREMIXED EQUATION

In non-premixed combustion, the fuel and oxidizer enter the reaction zone from different streams, in which reactants are mixed at the molecular level before burning. A Fluent Non-premixed combustion model was followed to estimate gaseous characteristics. The model simplifies the thermochemistry to the mixture fraction. By using this model species were determined from predicted mixture fraction quantities. Moreover, the relationship between turbulence and chemistry is modeled using a Probability Density Function (PDF). The PDF is computed before the simulation starts using the elements' initial conditions, which for this study is one gram of methane and four of oxygen. For this model the fluids were assumed to have equal diffusivities and compressibility effect, thus the species equations were condensed to a single mixture fraction function. Due to the fact that elements are conserved in chemical reactions, it is possible to cancel the reaction terms in the species equations. This assumption is typically suitable for turbulent flow only, as the turbulent convection overcomes molecular diffusion. This particular model was chosen due to the fact that it accounts for dissociation effects in the reaction allowing for flame temperature estimate. Theses equations are presented in Eqs. (6-8) [31]

$$f = \frac{Z_i - Z_{i,ox}}{Z_{i,fuel} - Z_{i,ox}} \tag{6}$$

$$\frac{\partial}{\partial t}(\rho\,\bar{f}\,) + \nabla \cdot (\rho \vec{v}\,\bar{f}\,) = \nabla \cdot \left(\left(\frac{k}{C_p} + \frac{\mu_t}{\sigma_t} \right) \nabla \bar{f}\, \right) + S_m + S_{user} \tag{7}$$

$$\begin{aligned} &\frac{\partial}{\partial t}\left(\rho\,\overline{\acute{f}^2}\right) + \nabla \cdot \left(\rho \vec{v}\,\overline{\acute{f}^2}\right) \\ &\qquad = \nabla \cdot \left(\left(\frac{k}{C_p} + \frac{\mu_t}{\sigma_t} \right) \nabla \overline{\acute{f}^2} \right) + C_g \mu_t . \left(\nabla \bar{f}\,\right)^2 - C_d \rho \frac{\varepsilon}{k}\,\overline{\acute{f}^2} + S_{user} \end{aligned} \tag{8}$$

$$\sigma_t = 0.85, \qquad C_g = 2.86\,, \qquad C_d = 2 \tag{9}$$

Table 3 Non-Premix Governing Equation Variables

Symbol	**Name**
Z_{fuel}	Mass Fraction of Fuel
Z_i	Elemental Mass Fraction for Element
Z_{ox}	Mass Fraction of Oxygen
f	Mixture Fraction
$\overline{f'^2}$	Mixture Fraction Variance
c_p	Mixture-Specific Heat
μ_t	Turbulent Viscosity
$\vec{v}$	Velocity
σ_t	Prandtl Numbers
k	Turbulent kinetic energy
ε	Dissipation rate
S_m , S_{user}	User-Defined Source Terms
C_g , C_d	Constant

2.3.4. ENERGY EQUATION

Heat transfer is a flow of thermal energy from matter occupying one region in space to matter occupying a different region in space. It occurs by three methods: conduction, convection, and radiation. The simplest physical models contain conduction and/or convection and ANSYS Fluent will solve a variation of the energy equation that takes into account the heat transfer methods that user has specified. When the non-adiabatic non-premixed combustion model is enabled, ANSYS Fluent solves the total enthalpy form of the energy equation (9). Under the assumption

that the Lewis number (Le) = 1, - where Lewis number defined as the ratio of thermal diffusivity to mass diffusivity and it is used to characterize fluid flows where there are simultaneous heat and transfer by convection- The conduction and species diffusion terms combine to give the first term on the right-hand side of equation (9) while the contribution from viscous dissipation appears in the non-conservative form as the second term. The total enthalpy *H* is defined as in Eq (10). Where Y_j is the mass fraction of species j and $h_j^0(T_{ref,j})$ is the formation enthalpy of species at the reference temperature $T_{ref,j}$

$$\frac{\partial}{\partial t}(\rho H) + \nabla . (\rho \vec{v} H) = \nabla . \left(\frac{k_{eff}}{C_p} \nabla H \right) + S_h \tag{10}$$

$$H = \sum_j Y_j H_j \tag{11}$$

$$H_j = \int_{T_{ref,j}}^{T} c_{p,j} dT + h_j^0(T_{ref,j}) \tag{12}$$

Table 4 Energy Governing Equations Variables

Symbol	**Name**
H	Total Enthalpy
v	Velocity
Y	Mass fraction
c_p	Mixture-Specific Heat
T	Temperature
μ_t	Turbulent Viscosity
$h_j^0(T_{ref,j})$	formation enthalpy of species at the reference temperature
S_h	the heat of chemical reaction and any other volumetric heat sources user defined.
t	Time
k_{eff}	Effective Conductivity

3. CHAPTER 3 COMPUTATIONAL DOMAIN AND EXPERIMENT

3.1. 2D Model

A fully-coupled axisymmetric 2D model including the combustion, wall and cooling domains was developed using Siemens NX and integrated into ANSYS FLUENT. The use of three domains in one simulation eliminates the necessity of iteration between heat flux and temperature in semi-coupled models. To account for the effect of wall heat conduction, material properties were adapted to those of Inconel 718 as temperature-dependent functions.

3.1.1. GEOMETRY

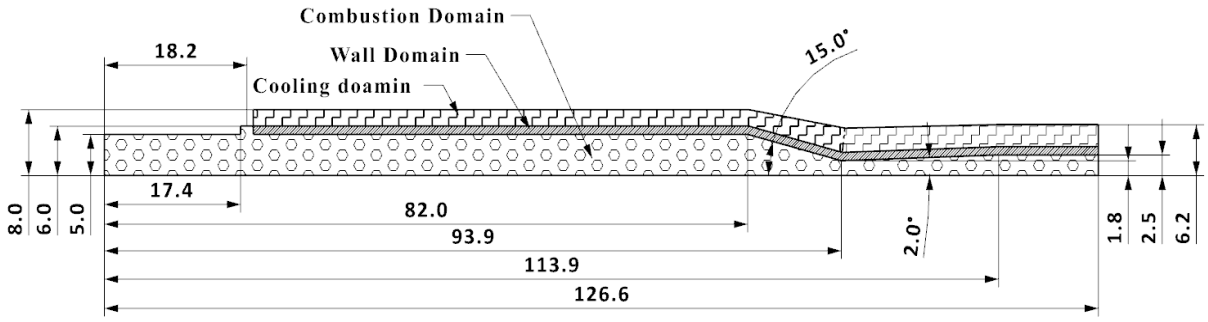

Figure 9 2D Model water/wall/combustor domains

As shown in Fig 9 the 2D model of water/wall/combustion dimensions are specified in mm. While the combustor's gaseous domain could be characterized as axisymmetric, fuel injection parameters required manipulation to characterize the geometry's original swirl coaxial configuration. Four fuel injection ports were converted into a ring with constant inlet velocity through the conservation of mass equation. The combustor gaseous domain dimensions are: oxidizer inlet is 10 mm.; fuel inlet is 1.8 mm.; throat is 3.8 mm.; exit is 5 mm.; converging nozzle angle is 15^{o} ; the diverging nozzle is 2^{o} ; The wall has a constant thickness of 1 mm. Channel geometry was modeled through the assumption of constant convective properties. Though the

physical model included support structures that helped maintain a constant hydraulic diameter, characterizing a steady gap in 2D will yield variable velocities. This is due to the changing nozzle shape: a 2-mm gap will not result in the same cross-sectional area in the throat as in the chamber. However, if the resulting channel area is maintained, the hydraulic diameter will not be constant due to the same reason.

A manipulation of a Nusselt-type correlation and the conservation of mass equation was performed to characterize the 2-D channel geometry in the profile. Equation 16 describes the rearranged Sieder-Tate correlation, where C is a constant that contains steady coolant properties and the required convective heat transfer coefficient. The hydraulic diameter is characterized as the difference between outer and inner diameters of an annulus. As such, cross-sectional channel area is described by equation 15 at any location of the channel. The conservation of mass equation is described by relationship 14. Density for this case is assumed to be steady due to the coolant being incompressible.

$$\rho_1 A_1 V_1 = \rho_2 A_2 V_2 \tag{13}$$

$$A = \frac{\pi}{4}\left({D_{OUT}}^2 - {D_{IN}}^2\right) \tag{14}$$

$$V = \left(\frac{D_{out} - D_{in}}{C}\right)^{.25} \tag{15}$$

3.1.2. MESH

Solving the governing equations stated in chapter 2 require transferring the geometry to smaller shapes. This transferring break down the complex geometry to a simple one. These simple shapes are used in the numerical technique for finding an approximate solution for the given engineering problem. Also, they are called elements and the process of generating these elements called meshing. There are many codes that generate the mesh, some of them are open sources and other and commercials. Usually, the open sources are difficult to use and not users friendly, but they allow customizing in the code. while the commercials codes are the opposite. Therefore, ANSYS Meshing -which is a commercials code- is used to generate the mesh for the 2D model.

Mesh metrics provide the mesh information and thereby evaluate the quality of the generated mesh in ANSYS Meshing. These mesh metrics are Element Quality, Aspect Ratio Jacobian Ratio, Warping Factor, Parallel Deviation, Maximum Corner Angle, Skewness and Orthogonal Quality. The parameters of importance for this thesis are Element Quality, Aspect Ratio, and Orthogonal Quality. The Element Quality provides a composite quality metric that ranges between 0 and 1. This metric is based on the ratio of the area to the sum of the square of the edge lengths for 2D quad/tri elements. The aspect ratio for a quadrilateral using only the corner nodes of the element. The aspect ratio of the quadrilateral is the ratio of a longer side of a shorter side of whichever rectangle is most stretched. The best possible quadrilateral aspect ratio, for a square, is one. Skewness is one of the primary quality measures for a mesh. Skewness determines how close to ideal (i.e., equilateral or equiangular) a face or cell is. According to the definition of skewness, a value of 0 indicates an equilateral cell (best) and a value of 1 indicates a completely degenerate cell (worst). The orthogonal quality for cells is computed using the face normal vector, the vector from the cell centroid to the centroid of each of the adjacent cells, and the vector from

the cell centroid to each of the faces. The range for orthogonal quality is 0-1, where a value of 0 is the worst and a value of 1 is best [32].

The mesh is presented in Figure 10. The mesh controls are the flowing. Face sizing is applied to the three bodies with face sizing of 0.1 mm. Also, face meshing is applied to the three bodies to make the mesh structured. The mesh metric is summarized in Table 5.

Table 5 2D Mesh Metric summary

Nodes			82243	
Elements			78727	
Mesh Metric	Min	Max	Average	Standard Deviation
Element Quality	0.710	0.999	0.939	0.041
Aspect ratio	1.000	1.900	1.302	0.202
Orthogonal Quality	0.953	1.000	0.998	0.005
Skewness	0.000	0.199	0.026	0.032

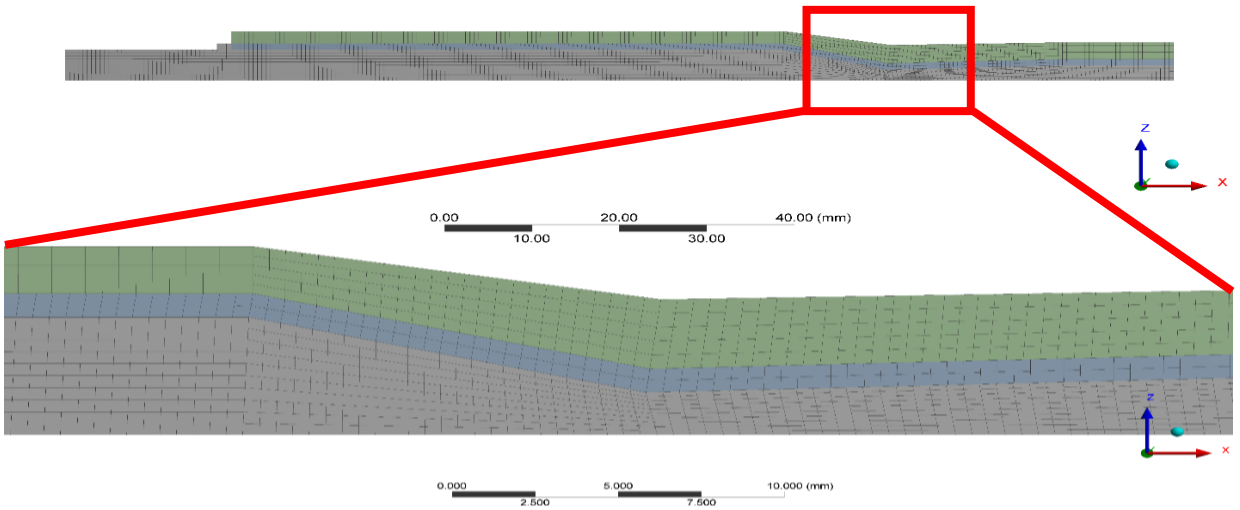

Figure 10 2D Model Mesh

3.1.3. BOUNDARY CONDITIONS

The boundary conditions employed for this model are summarized in Table 6.

Table 5 2D Model Boundary Conditions

Section	Input
General -Solver	❖ Type: Pressure-Based ❖ Velocity Formulation: Absolute ❖ Time: Steady ❖ 2D Space: Axisymmetric
Models	❖ Energy-ON ❖ Viscous: Realizable k- ε, Standard k-epsilon, ❖ Species: non-premixed combustion ➢ Inlet diffusion-ON ➢ Compressibility effects-ON ➢ Fuel stream rich flammability limit- .28 ➢ Mass fraction of CH4-1 ➢ Mass fraction of O2-1
Materials	❖ PDF Mixture ❖ Inconel 718 ➢ Custom density 8190 kg/m3 ➢ Custom Cp 435 J/kg-k ➢ Thermal conductivity function ❖ Liquid Water
Boundary Conditions	❖ Fuel Inlet: Mass flow rate ➢ Hydraulic diameter- 1.8 mm ➢ Mean mixture fraction -1 ❖ Oxidizer inlet: Mass flow rate ➢ Hydraulic diameter- 10 mm ❖ Gas outlet: Pressure outlet ➢ Atmospheric pressure (initial) ❖ Water inlet: Velocity Outlet ➢ Velocity-17.6 m/s ➢ Gauge Pressure 1310 KPa [190 psi] ❖ Water outlet: Pressure Outlet ➢ Atmospheric pressure (initial)
Solution Initialization	Standard-Oxidizer Inlet

In the solution methods, the scheme of pressure and velocity was performed through the COUPLED algorithm. which solves the momentum and pressure-based continuity equations together. The coupled scheme obtains a robust and efficient single phase implementation for steady-state flows, with superior performance.

To get the results to converge the spatial discretization for variables changed to first order and change the pressure to the liner. Then the calculation run for 200 iterations. After that, the pseudo-transient activated with a time step of 0.0001s for solid and fluid domains. Then the calculation was performed again.

3.2.3D Model

The purpose of this model is to account for the geometrical irregularities not present in the 2-D model, including sensor ports and channels region. A three-dimensional geometry is made combustor wall and coolant domains as it shown in Figure 11. This design simulates the real MHD combustor. Like in the 2-D simulation, the effects of the super alloy's properties were replicated through the introduction of temperature-dependent properties in the material. The 2-D wall heat flux was characterized as a profile and introduced as a boundary condition on the inner wall of this

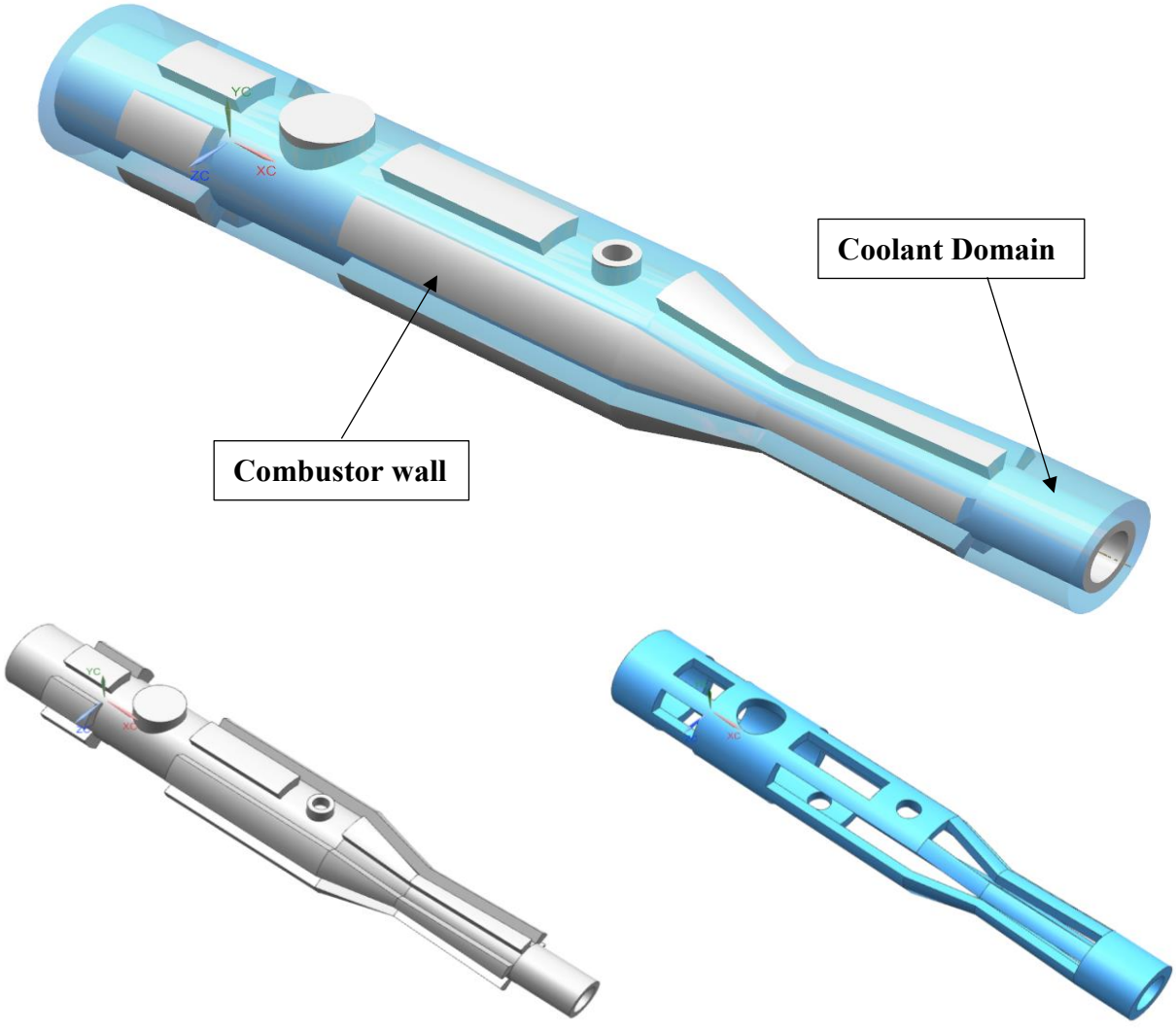

Figure 11 3D Model of water and combustor domain

combustor wall.

3.2.1. GEOMETRY

As shown in Fig 12 the 3D model of combustion wall and coolant domain dimensions are presented and all dimensions are specified in mm. Also, two sections - B-B and C-C – are made in the combustion wall and coolant domain to show the interior dimensions. The obstruction caused by the instrument and sensors are presented in addition to cooling channels. These

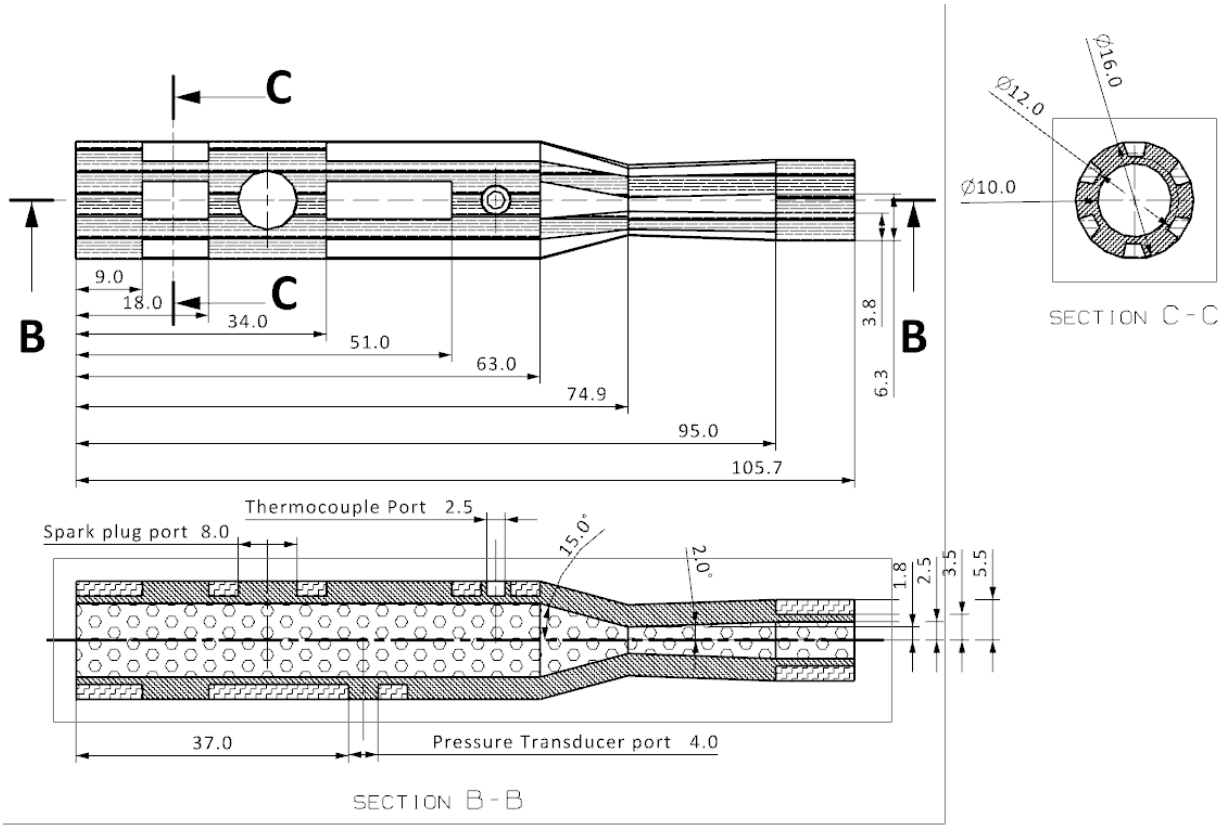

Figure 12 3D Model water and combustor domain

obstructions and channels are added to make the model more realistic case and study the stagnation regions and their effects on the flow.

3.2.2. MESH

Similar to what have been stated in section 3.1.2., a mesh is also required for the 3D model. Using the same approach of mesh 2D model. The final 3-Dmesh is presented in Figure 13. The mesh method is tetrahedrons. This method is used because of the complex geometry. Also, mesh controls of body sizing of 0.1 mm. This sizing is applied to the two domains. In addition,

the size function of proximity and curvature ,and the relevance center is fine. These methods are used to increase the elements quilt around the edges and curvatures.

Table 6 3D Mesh Metric summary

Nodes		282549		
Elements		1356948		
Mesh Metric	Min	Max	Average	Standard Deviation
Element Quality	0.113	1	0.838	0.095
Aspect ratio	1.158	15.394	1.856	0.457
Orthogonal Quality	0.122	0.995	0.857	0.0814
Skewness	0.000	0.895	0.227	0.12

Figure 13 3D Model Mesh of water and combustor domain

3.2.3. BOUNDARY CONDITIONS FOR 3D MODEL

The boundary conditions employed for this model are summarized in Table 7.

Table 7 3D Model Boundary Conditions

Section	Input
General -Solver	❖ Type: Pressure-Based ❖ Velocity Formulation: Absolute ❖ Time: Steady
Models	❖ Energy-ON ❖ Viscous: Realizable k- ε, Standard k-epsilon.
Materials	❖ Inconel 718 ➢ Custom density 8190 kg/m3 ➢ Custom Cp 435 J/kg-k ➢ Thermal conductivity function ❖ Liquid Water
Boundary Conditions	❖ Combustor inner wall: imported heat flux from 2D model ❖ Water inlet: Velocity Outlet ➢ Velocity-17.6 m/s ➢ Gauge Pressure 1310 KPa [190 psi] ❖ Water outlet: Pressure Outlet ➢ Atmospheric pressure (initial)
Solution Initialization	Standard-Oxidizer Inlet

Similar to 2D boundary conditions in the solution methods, the scheme of pressure and velocity was performed through the COUPLED algorithm. Spatial discretization for the pressure choose to be PRESTO and the rest variables are second order upwind.

3.3.Experimental cases

The purpose of the experiments was to obtain an experimental data for temperature. The pressure measurements were gain from water inlet and outlet and the temperature measurements were gain from water inlet and outlet and also from the combustor external wall.

The obtained data gained from running the experiment for 5 minutes. NASA Chemical Equilibrium with Applications code was used to estimate the theoretical operating fuel and

oxidizer mass flow rate at theoretical pressure. After the flow rate is set by setting the propellants tank to the desired pressure, also water flow rate was maintained constant at 17.8 LPM throughout the tests. Combustion occurred in all cases for five minutes to emulate steady-state operation.

To calculate the heat flux, Data obtained from the water inlet and outlet and combustor wall are used to calculate the heat flux. This data is imported to Matlab and coded to calculate the heat flux. First, the water inlet and outlet temperatures are averaged. then the density, thermal conductivity, specific heat, and dynamic viscosity are calculated with respect to the water average temperature. After that dynamic viscosity are calculated with respect to the wall temperature. Then convective heat transfer coefficient is calculated. Finally, the heat flux is calculated using convective heat transfer coefficient and the difference of the averaged water temperature and combustor wall temperature.

4. CHAPTER 4 RESULTS AND DISCUSSION

4.1.2D Results

4.1.1. 2D RESULTS

As expected from theory Figure 14 shows the static temperature contours for the 2-D coupled simulation. The mixing region can easily be recognized in the temperature contour.

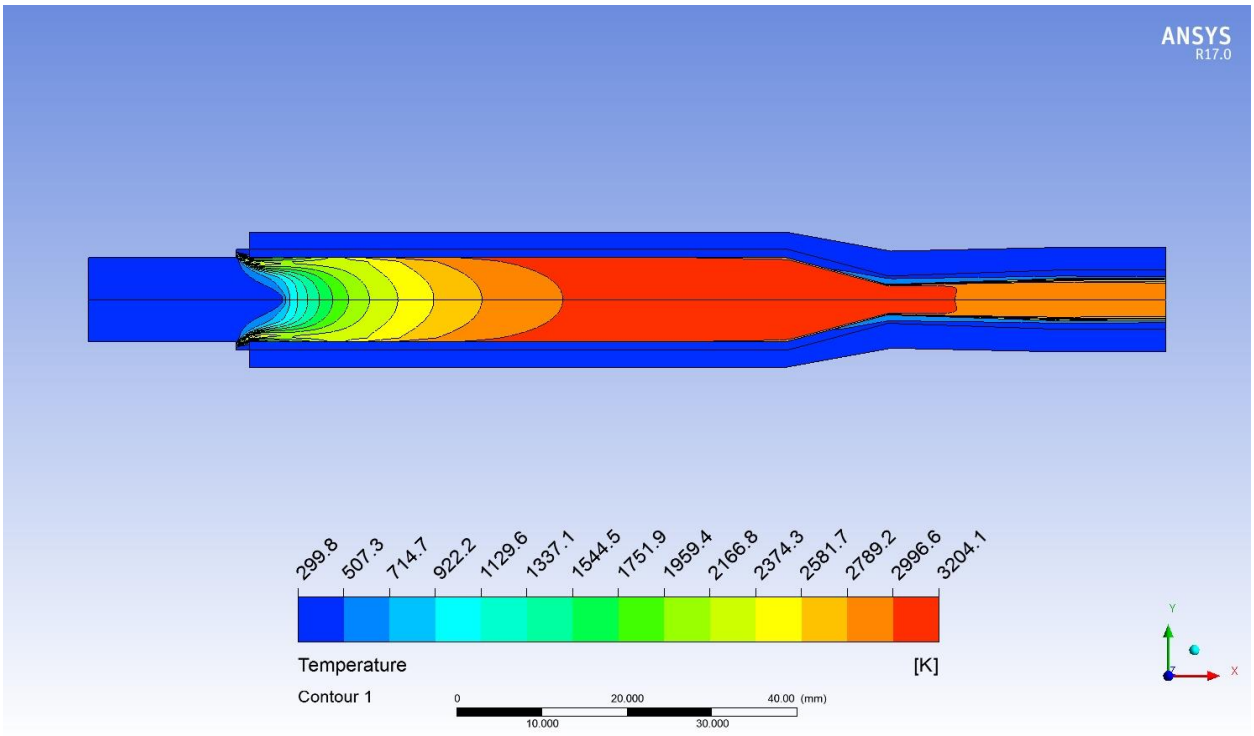

Static Temperature Contour of combustor domain [A]

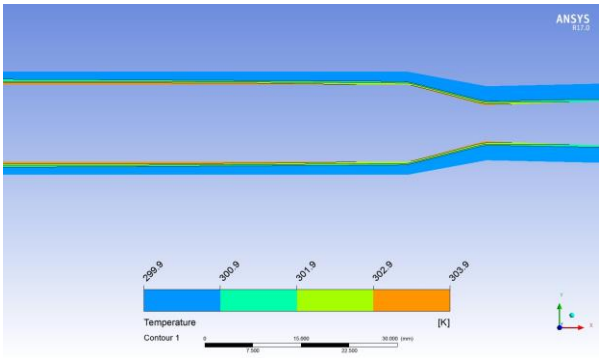

Static Temperature Contour of water domain [B]

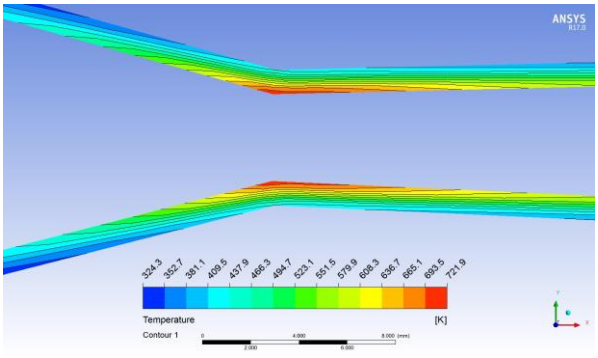

Static Temperature Contour of wall domain [C]

Figure 14 2D Static Temperature Contour

Shortly after the methane injector ports temperature increases very rapidly, reaching up to 3204 K at the combustion chamber. The temperature then decreases again in the diverging section of the nozzle. The exit temperature is the range of 2789 and 2996 K. As it shown in Figure 14 [A], Static Temperature Contour of water domain is shown in Figure 14 [B]. The water temperature is maximized at the throat with 303.9 K. Static Temperature Contour of wall domain is shown in Figure 14 [C].

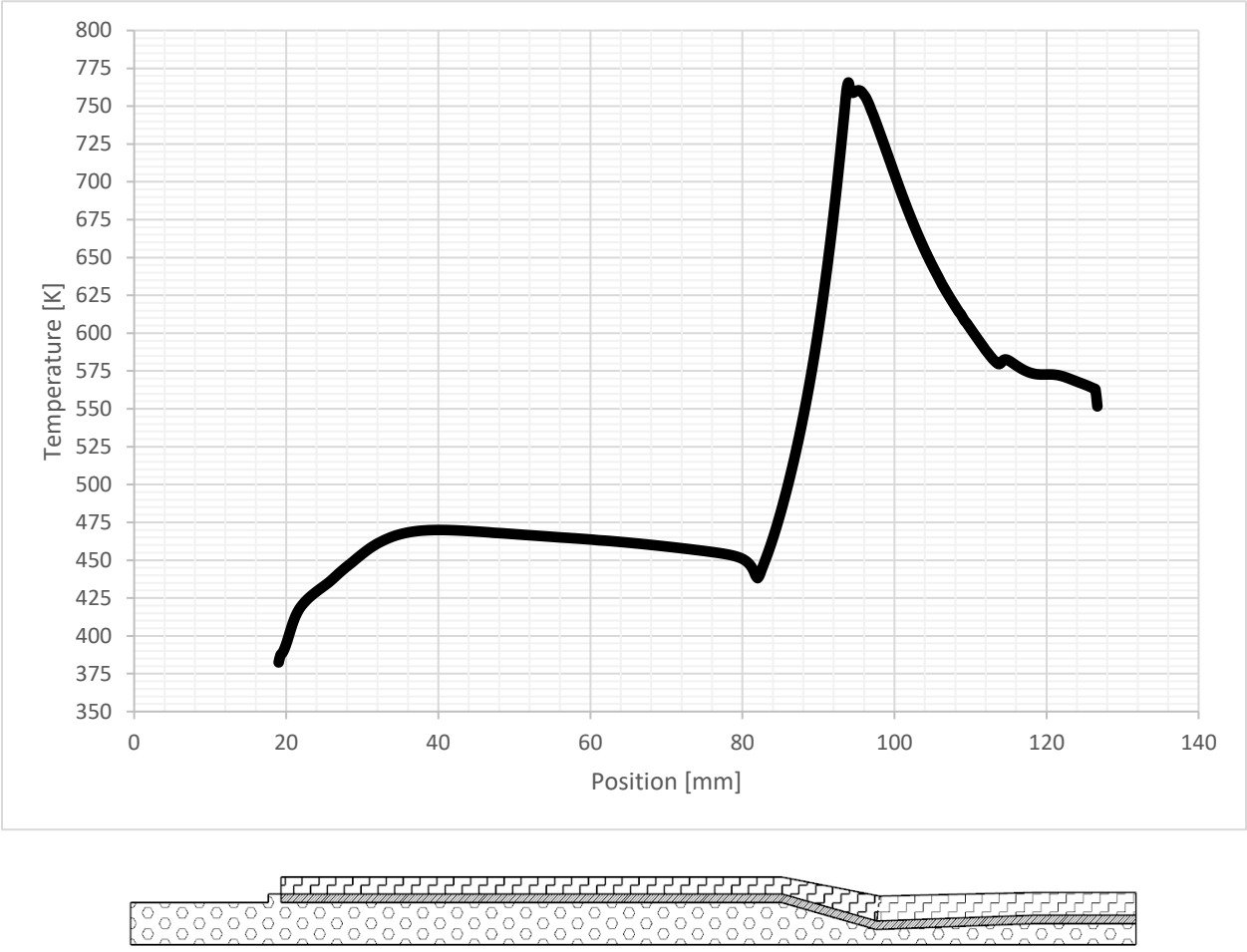

Plot 1 2D model Temperature at the inner combustor wall

The wall temperature also is maximized at the inner wall of the throat with 765.7 K. Plot 1 shows the temperature distribution of the combustor wall in respect to X Axis. As it shown,

the temperature at the combustor wall at the chamber ranges from 375 to 475 K. and at the nozzle it ranges from 430 to 765 K.

. The heat flux at the inner wall of the combustor is presented on plot 1. The maximum heat flux located at the throat and it is 7.5 MW/m^2. The averaged heat flux of the Chamber is 1.8 Mw/m^2.

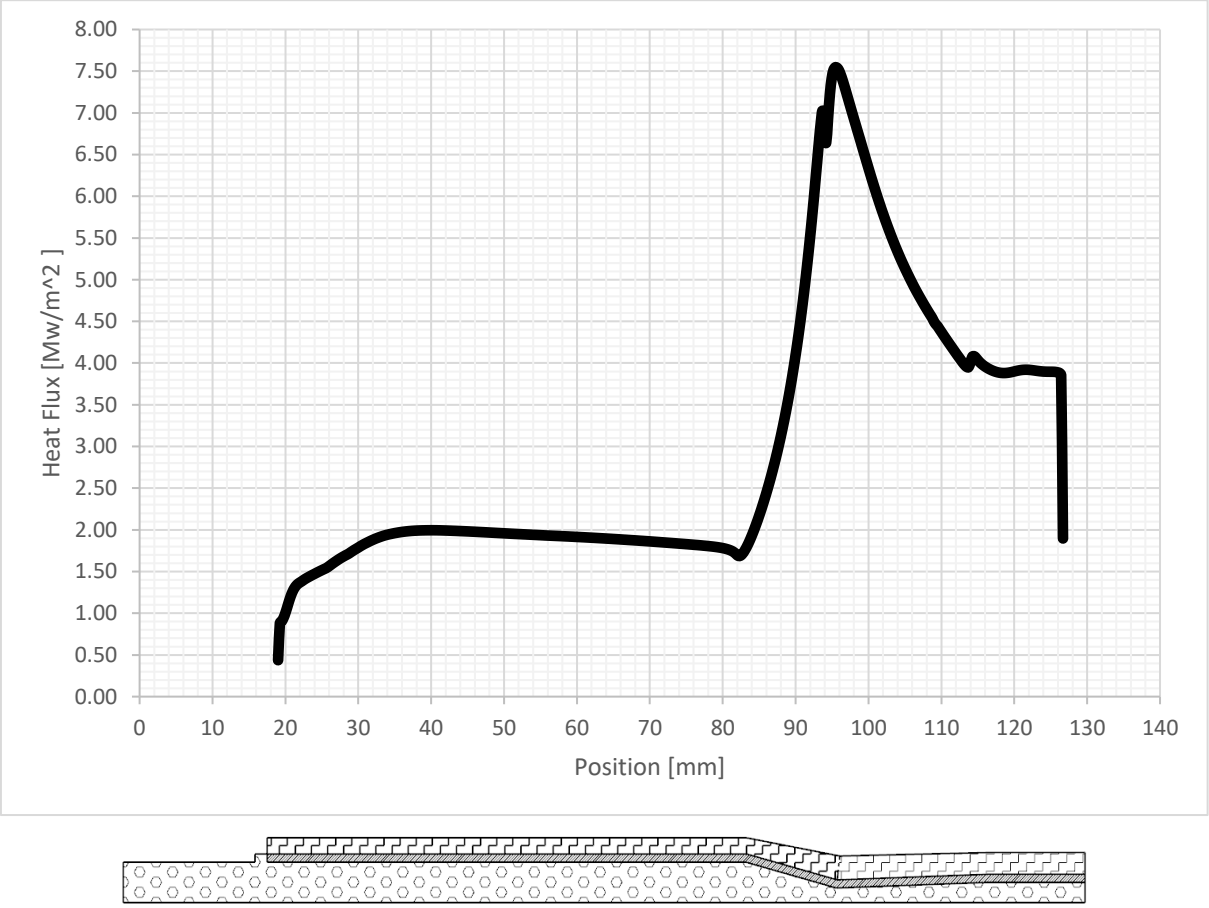

Plot 2 Heat Flux at the combustion wall

4.1.2. 2D RESULTS DISCUSSION

Even though the same boundary conditions were specified in both programs, it had been anticipated that Fluent's results would be more realistic and therefore lower. The basis for that prediction was that CEA is a one-dimensional isentropic case, contrary to Fluent which is a

three-dimensional model that takes into account other factors such as thermal and friction losses.

Temperature results have been tabulated in Table 8 against those estimates generated by the NASA's CEA code and analytical calculations. The model's estimates for gaseous properties present a variation of less than 10% when compared to the isentropic flow relations within the CEA code and analytical calculations.

Table 8 2D results summary

Parameter	Symbol	2-D CFD	NASA CEA	Error	Units
Chamber Temperature	T_c	3204	3315	3%	K
Exit Temperature	T_e	2892	2873	1%	K
Heat flux at the throat	q'	7.5	7.3	2.5%	Mw/m^2

4.2. 3D Results

4.2.1. COMBUSTOR INNER WALL

After the heat flux was applied to the combustor wall in the 3D Model, temperature contour for the coolant and combustor was obtained. Figure 15 shows the temperature counters of combustor inner and external walls respectively. The highest temperature of 1056K was reached at the throat. This temperature corresponds to maximum heat flux profile that is located at the throat. This temperature is higher than the designed temperature within 20%. Therefore, further more investigation should focus on the throat mesh and the fluent model. The channels displayed a temperature range of 500-760K. This can be contributed to the lower heat flux encountered in the chamber region. The particular areas of interest were in the chamber where obstructions were placed for the static pressure and temperature measurement devices. These

areas were of high interest because they would obstruct the flow of the water and decrease its velocity, providing the opportunity for hot spots and cavitation to occur within the channels.

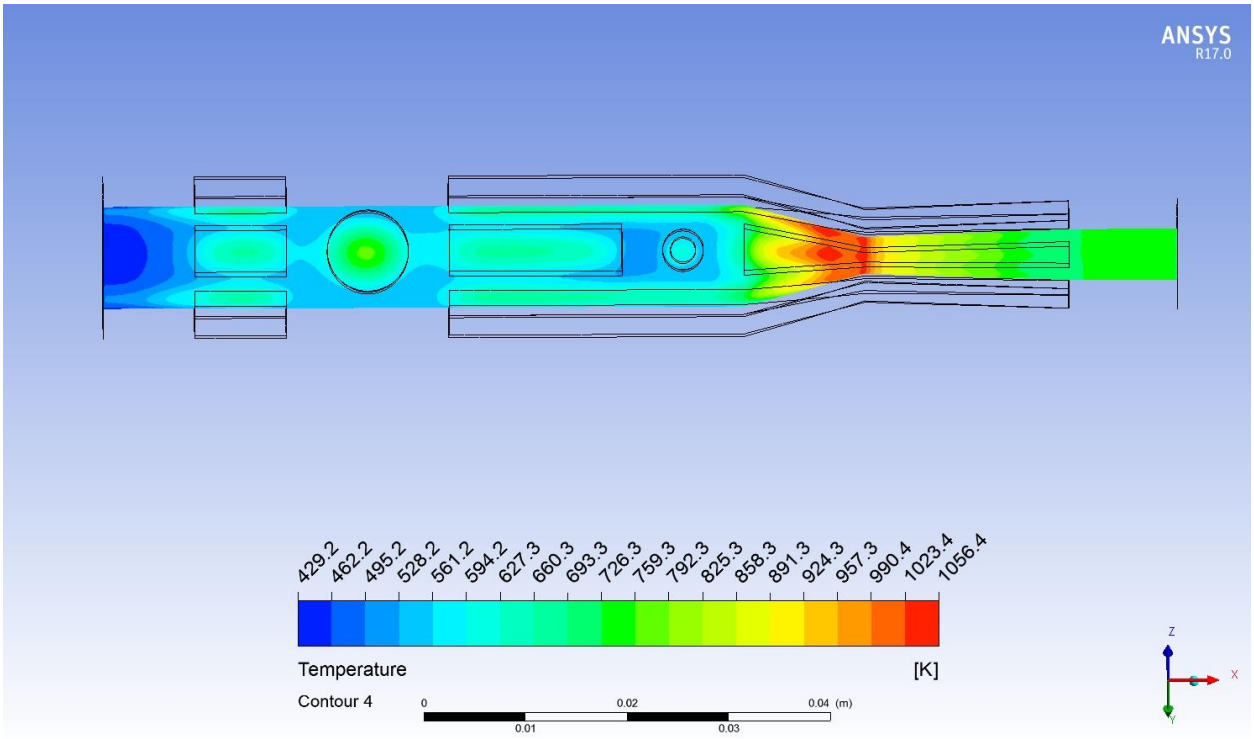

Figure 15 3D Model inner wall combustor temperature

4.2.2. COMBUSTOR EXTERNAL WALL

Figure 16 presents the temperature contour for the combustor external wall. It is determined that the highest temperature of 719K was reached at the combustor exit. The highest temperature is observed at that region because this area does not contain any channels. Therefore, it decreases the heat transfer rate. As demonstrated in the image, the temperature begins to decrease upstream up to the injection point. This can be contributed to the lower heat flux encountered in the chamber region.

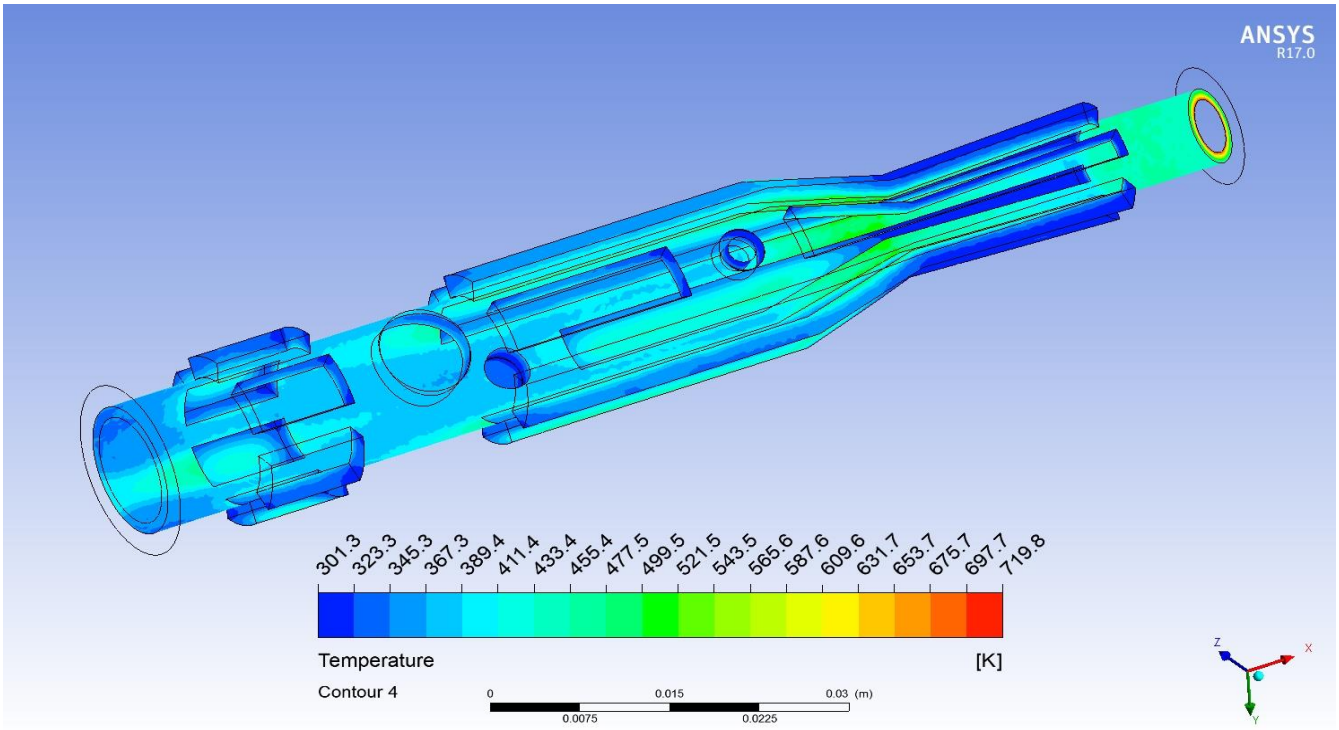

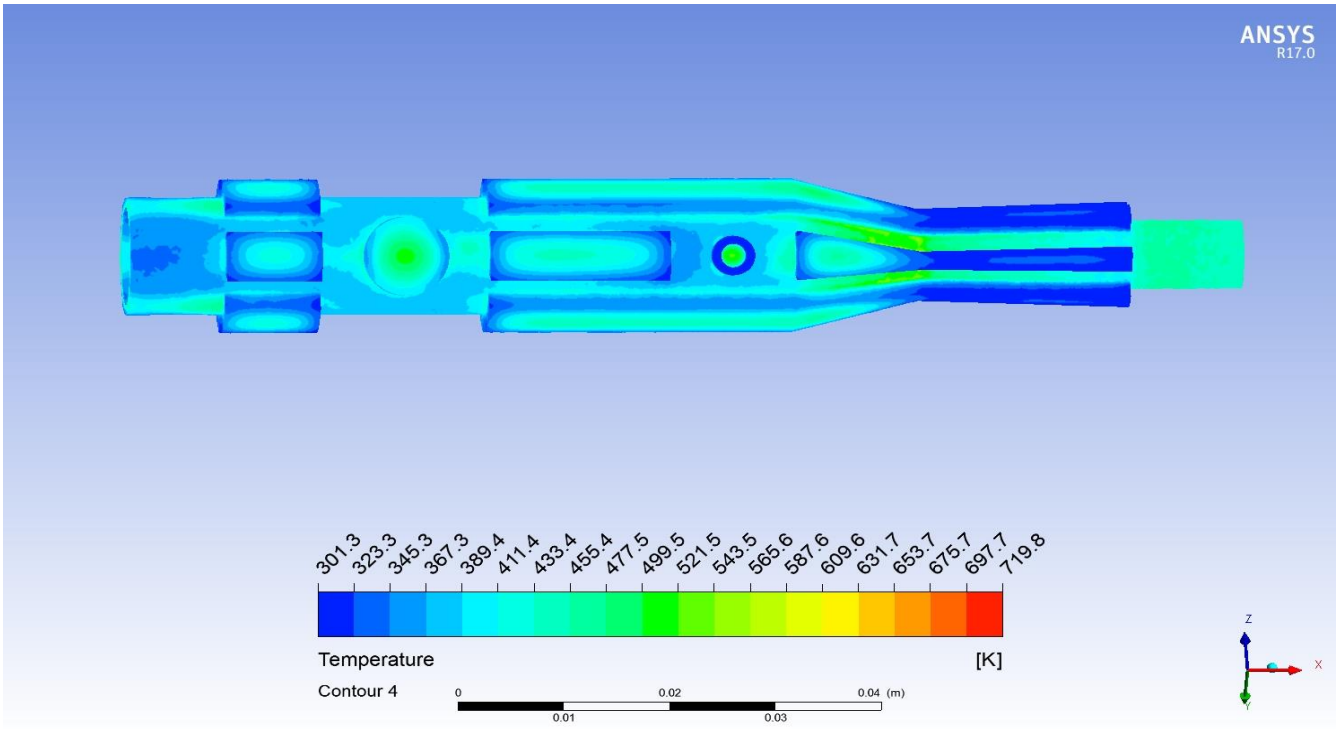

Figure 17 3D Model external combustor wall temperature

4.2.3. COOLANT DOMAIN

Figure 17 presents the coolant Domain It is determined that the highest temperature of 517K was reached at the throat where the coolant domain and the combustor are in contact. The highest temperature is observed at that region because it corresponds the maximum heat flux. As demonstrated in the image, the temperature increases at the regions that do not have channels and where the obstructions are located. This can be contributed to the heat flux profile and coolant velocity changes in these regions.

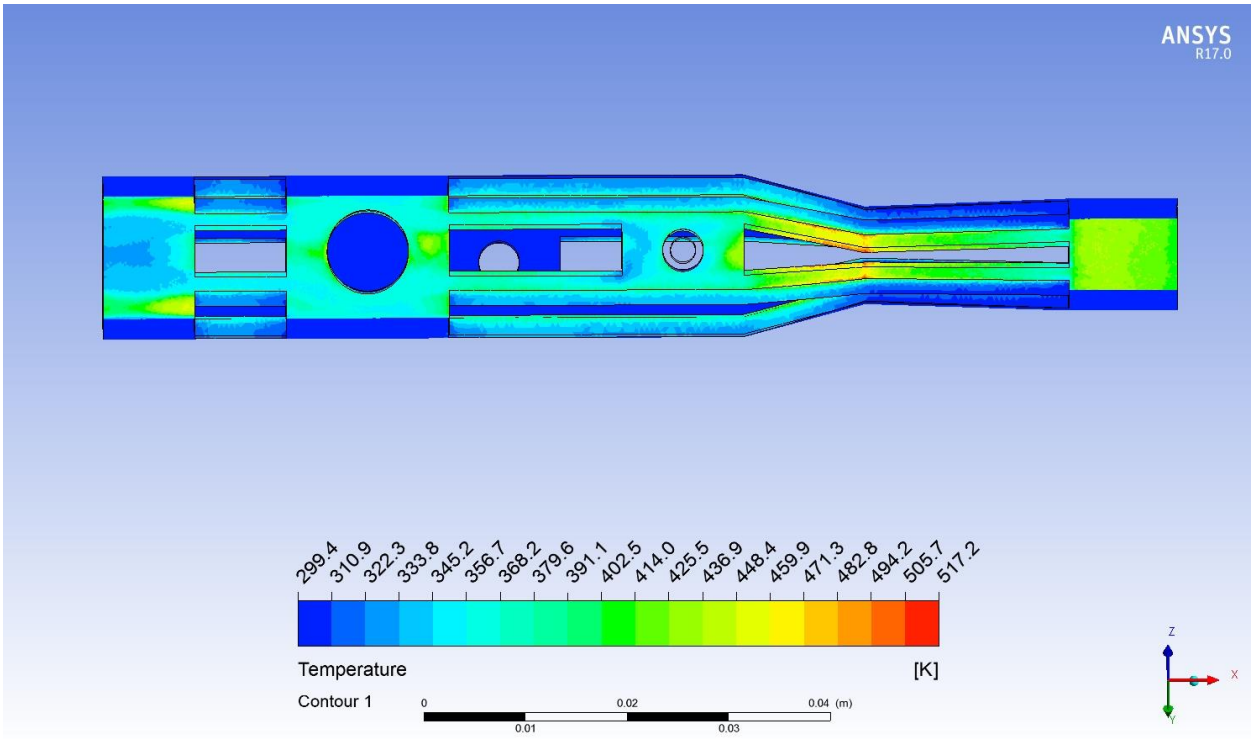

Figure 18 3D coolant domain temperature

Temperature data from Fluent is expert to excel to be plotted. After an average function in excel been applied the results is presented in Plot 3. Plot 3 shows the averaged surface temperature in the contact region between the combustor and coolant domain. As it stated before, the temperature increases at the regions that do not have channels and where the

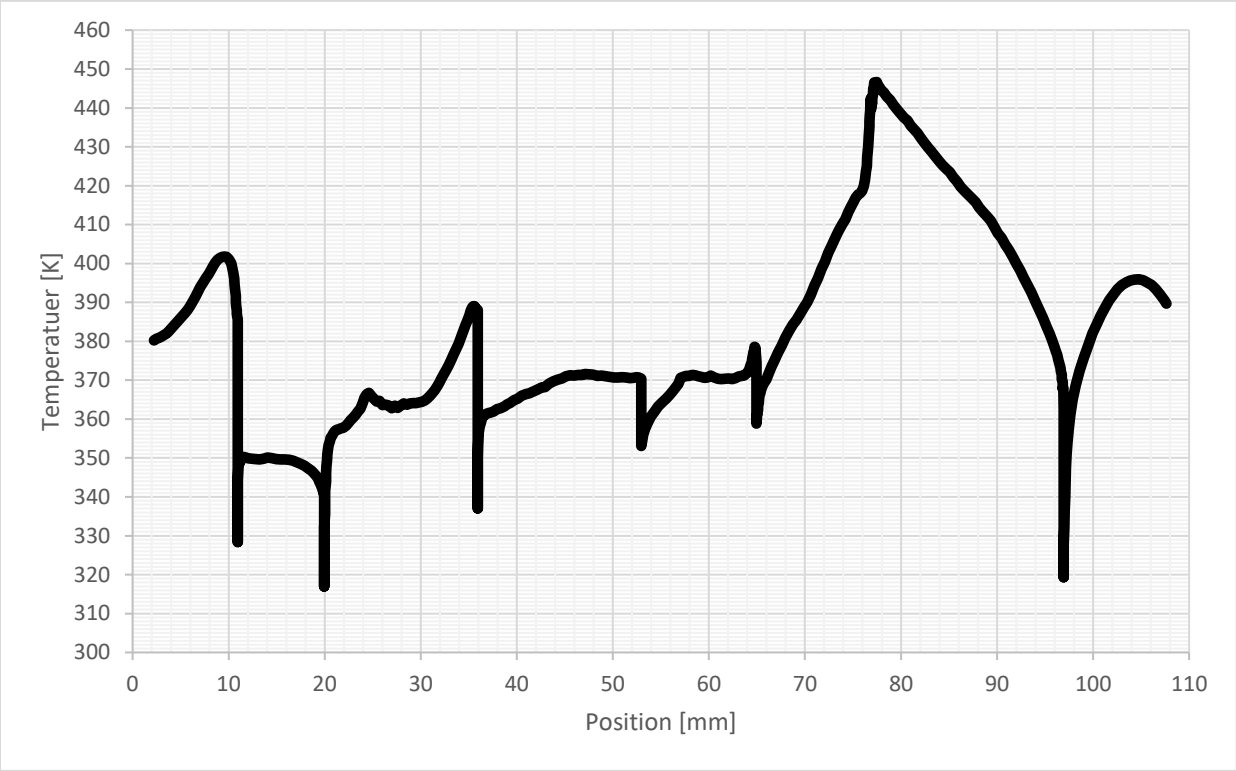

Plot 3 3D Combustor Channels Temperature

obstructions are located. The maximum temperature is located at the nozzle. Also, the temperature of 370K is measured where the thermocouple is located.

In addition to the surface temperature, ANSYS Fluent is used through Surface Integral Report to measure the difference between the water outlet and inlet temperature as in shown in Table 9

Table 9 The temperature Difference between the coolant outlet and inlet

Area-Weighted Average	water inlet	water outlet
Static Temperature [k]	300	303.2

Similarly, to temperature, Heat flux data from Fluent is expert to excel to be plotted. After an average function in excel been applied the results is presented in Plot 4. Plot 4 shows the averaged surface Heat flux on the contact region between the combustor and coolant domain. The maximum heat flux is located at the nozzle. Also, the heat flux of 1.85 Mw/m^2 is measured where the thermocouple is located.

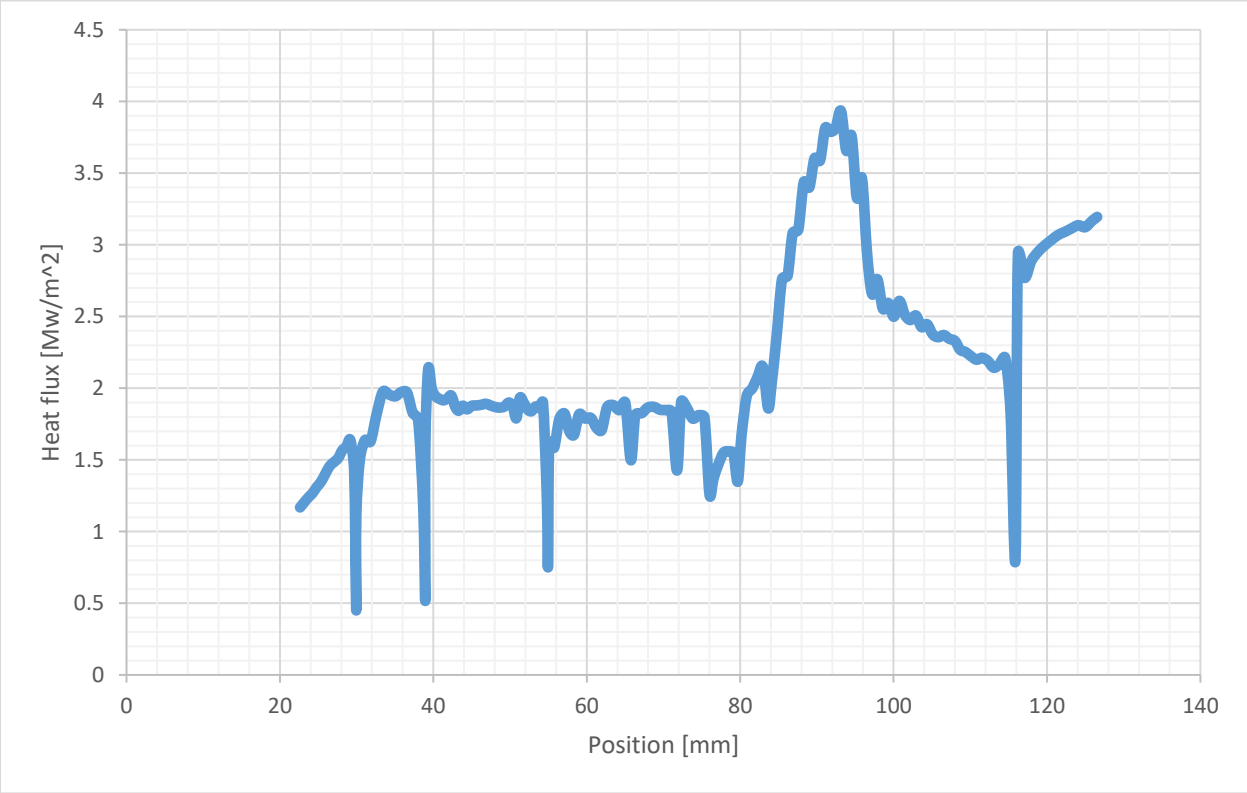

Plot 4 3D Combustor Channels Heat flux

4.3.Experimental results

The experiment run for 300 secs with the conditions listed in table 10

Table 10 Testing conditions

	Coolant	Oxidizer	Fuel
Flow rate [LPM]	17.8	150	80

4.3.1. COOLANT AND WALL TEMPERATURE

Plot 5 presents the coolant inlet, and outlet and combustor wall temperature plot with respect to time. As it shown in plot 5, the combustor wall temperature increased after the combustion occurred at 7 seconds from the ambient temperature of 302K (29 C^{o}). After 25 seconds the wall

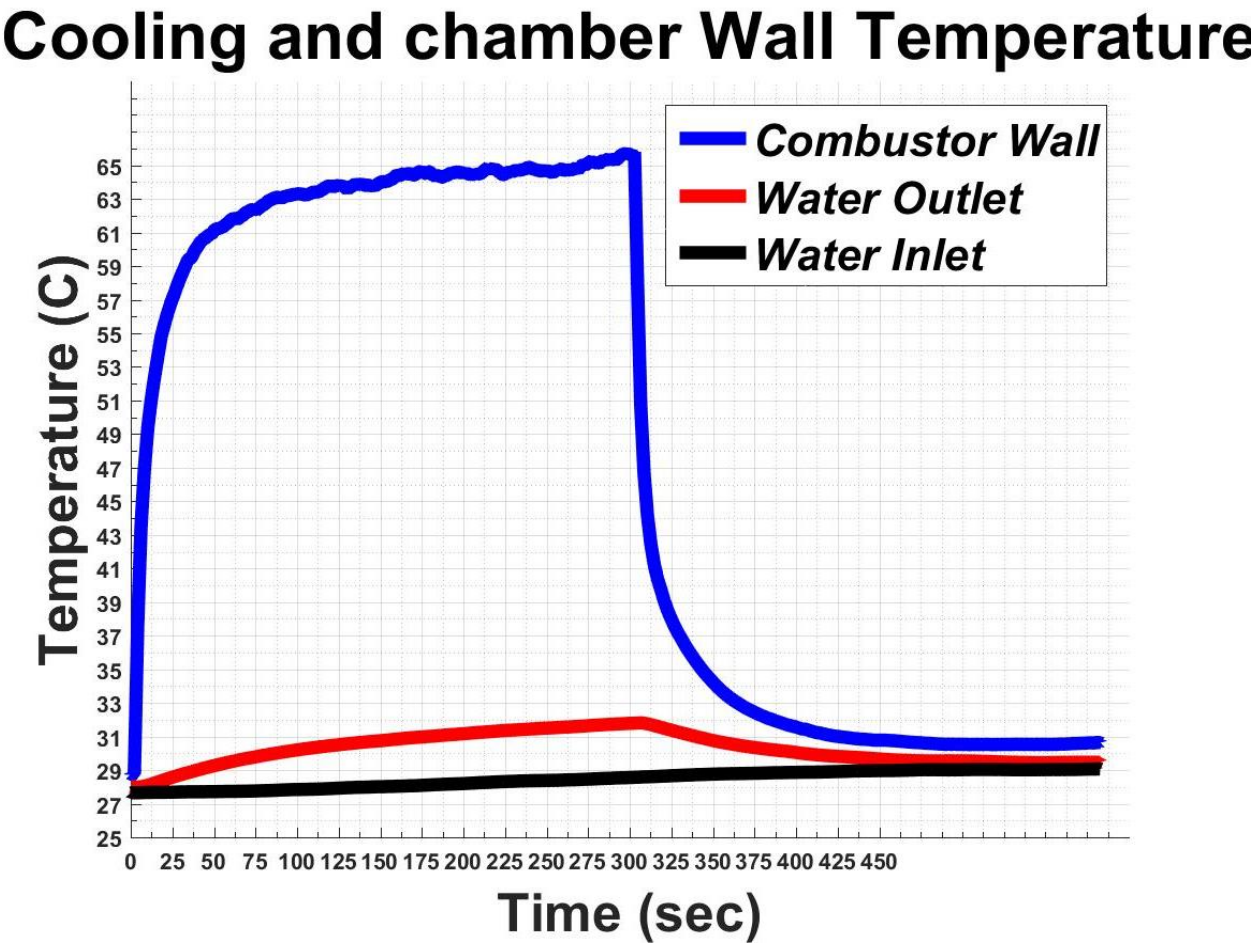

Plot 5 Coolant and chamber wall Temperature

temperature starts to stabilize and reached 331K (59 C^{o}). Then the temperature increases slowly to

reach 338K (65 Cº). after 300 seconds. This increase of 6 degrees over the 225 second could consider as steady-state operation. The temperature of the experiment results is Compared to CFD temperature results of the 3D model at the same region stated in Plot 3. The difference between these results is 8.6%. The water outlet temperature increases after 20 seconds. The maximum temperature of 305.65K (32.5 Cº). is reached after 275 seconds. The water inlet temperature starts increasing slowly during the experiment because the water is reused during the experiment without cool it down to the ambient temperature.

4.3.2. WATER TEMPERATURE DIFFERENCES

Plot 6 present the Coolant Temperature difference between outlet and inlet. As it shows,

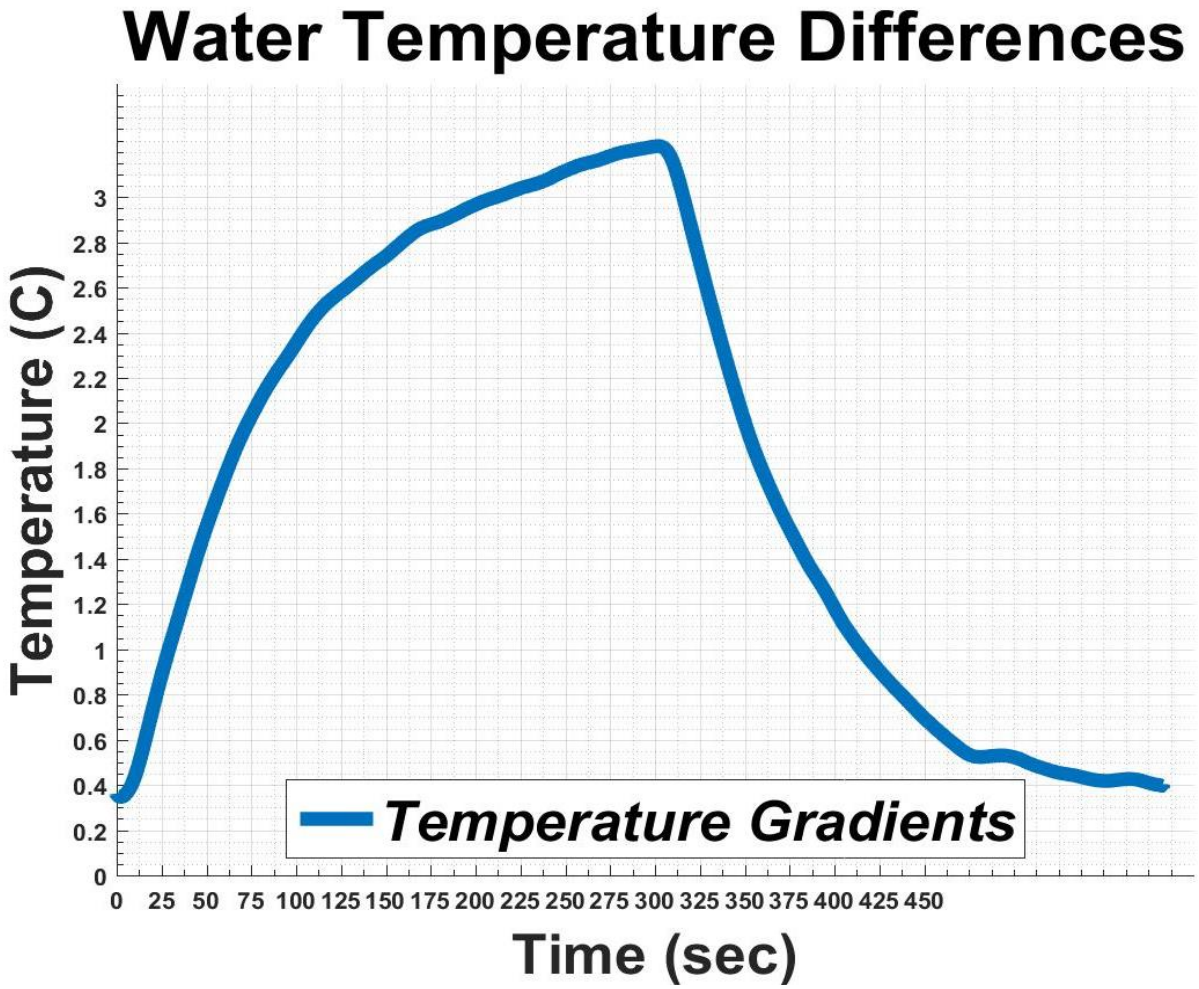

Plot 6 Coolant Temperature differences

the difference of 3.25 degree. Comparing this results with the one obtained from the CFD results stated in Table 9, the different is calculated to be 1.5%.

4.3.3. HEAT FLUX AT THE THERMOCOUPLE PORT

Plot 7 present the heat flux at the thermocouple port. As it shows heat flux reached near steady state operation during the test with maximum heat flux of 1.7 Mw/m^2

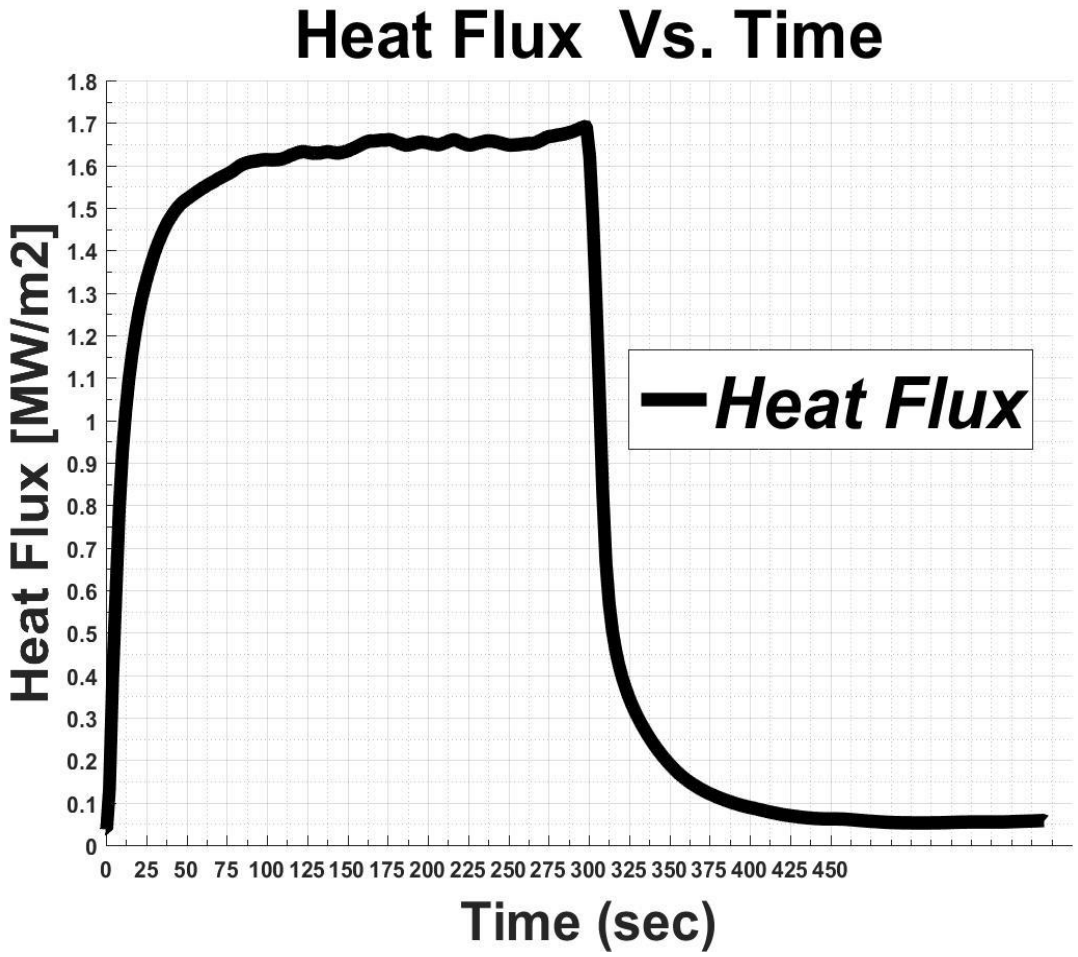

Plot 7 Heat Flux

Comparing this results with the one obtained from the CFD results stated in Plot 4, the different is calculated to be 8.5%.

5. SUMMERY AND CONCLUSION

Recent interest in efficient and low-pollution power generation has led to an investigation of various energy producing devices. A technology that lost attractiveness among investors in the 20th century and now being revisited is Magnetohydrodynamics (MHD). MHD power generators extract electrical energy directly from gasses flowing through a magnetic field. Some advantages of these systems include:

- No mechanical components, therefore higher efficiency.
- Potential to reach higher efficiencies than those of coal burning due to a higher temperature.
- Higher thermal efficiencies associated with oxy-fuel combustion.
- The combustion Products are only H_2O and CO_2, therefore, the system eliminates toxic combustion, also the CO_2 can be sequestered.
- MHD generators can be retrofitted into existing power plants, using the exhaust gasses as an energy source to generate steam.

Some of the disadvantages are:

- Producing pure oxygen requires a lot of energy
- MHD generators are still in early stages and need more development
- Effective cooling system is required to achieve high temperature

For this Thesis, computational fluid dynamic modeling of DPE MHD cooling system is used to build DPE MHD combustor and then compare the modeling resulting with experimental data are presented. The computational fluid dynamic modeling includes coupled system of 2D and 3D model. The main findings from this study are:

- In the 2D model, both the temperature of chamber and nozzle exit of 3204K and 2892K were successfully achieved with the combustor. Data from NASA CEA and Fluent matched within 3% and 1%, respectively. Also, a full combustion occurred and generated a heat flux profile correspond to geometry profile. This heat flux profile has a maximum value of 7.5 Mw/m^2 and it is located at the throat. And matches the analytical calculation within 2.5% error.
- In the 3D model, the combustor inner wall temperature corresponded to the heat flux profile and reached a maximum at the throat with a temperature of 1058K which is higher the designed temperature by 20%. Therefore, further investigation on the mesh and fluent model to improve the modeling accrue. On the other hand, other parameters like temperature and heat flux at the thermocouple port match the experimental within 10% error.
- In the experimental result,

While developing the various simulations, it was always useful to start with a basic model and gradually add details making it more accurate. The simplicity of these models made it possible to validate Fluent's results by hand, proportioning confidence on the results of their more complex counterparts. They also permitted to freely explore different combinations of boundary conditions to find the ones that worked best.

In conclusion, coupling model that been used in this thesis between 2D and 3D simulation is a valid approach, because most of the CFD result match the experimental data. As a reason, this methodology will be used to design 1MW combustor with improvement for the mesh and CFD models.

REFERENCES

[1] "Powering a generation of change," July 2014. [Online]. Available: http://americanhistory.si.edu/powering/index.htm.

[2] L. F. Drbal, P. G. Boston and K. L. Westra, Power plant engineering., New York, NY 10013 : Springer Science & Business Media, Inc., 2012.

[3] "Greenhouse Gas Emissions," 15 April 2016. [Online]. Available: https://www.epa.gov/ghgemissions/us-greenhouse-gas-inventory-report-1990-2014.

[4] "Human Health and Environmental Effects of Emissions from Power Generation," 2014. [Online]. Available: https://www.epa.gov/captrade/documents/power.pdf. [Accessed 2016].

[5] "RENEWABLE & ALTERNATIVE FUELS," 28 June 2011. [Online]. Available: http://www.eia.gov/renewable/annual/preliminary/index.cfm.

[6] "Today in Energy," 1 July 2016. [Online]. Available: http://www.eia.gov/todayinenergy/detail.cfm?id=26912.

[7] V. Malghan, "History of MHD power plant development," *Energy Conversion and Management,* vol. Volume 37, no. Issue 5, pp. Pages 569-590, May 1996.

[8] M. . N. Sadiku, Elements of Electromagnetics, New York: Oxford University Press, 2007, p. 386.

[9] T. E. o. E. Britannica, "Magnetohydrodynamics (MHD)," [Online]. Available: https://www.britannica.com/science/magnetohydrodynamics.

[10] A. K. R and J. B. S, "Magnetohydrodynamic Power Generation," *International Journal of Scientific and Research Publications,* pp. 1-11, 2013.

[11] N. Kayukawa , "Open-cycle magnetohydrodynamic electrical power generation: a review and future perspectives," in *Progress in Energy and Combustion Science 30.1*, 2004.

[12] J. F. L. R. J. R. a. Z. J. J. S. T. R. Brogan, "A REVIEW OF RECENT MHD GENERATOR WORK AT THE AVCO-EVERETT RESEARCH LABORATORY," 1962.

[13] D. TANAKA and Y. HATTORI, "Characteristics of Resistive Electrode in MHD Generator Duct and a Minimizing Technique for Internal Power Loss," *Journal of Nuclear Science and Technology,* vol. 14, no. 4, pp. 247-256, 1977.

[14] R. J. Rosa, C. H. Krueger and S. Shioda, "Plasmas in MHD Power Generation," *IEEE TRANSACTIONS ON PLASMA SCIENCE,* vol. 19, no. 6, pp. 1180 - 1190, DECEMBER 1991.

[15] R. C. Murray, S. H. Zaidi, M. R. Carraro, L. Vasilyak, S. O. Macheret, M. N. Shneider and R. B. Miles, "Observation of MHD Effects with Non-Equilibrium Ionization in Cold Supersonic Air Flows," *AIAA Aerospace Sciences Meeting and Exhibit,* 2004.

[16] M. J. Hernandez, L. A. Cabrera, O. Vidana, M. Chaidez and N. D. Love, "Design of a Supersonic Oxy-Methane Combustor for Direct Power Extraction," *54th AIAA Aerospace Sciences Meeting,* p. 8, Januery 2016.

[17] E. P. Velikhov, V. D. Pismenny, A. V. Pisakin, B. B. Zhukov and E. M. Sukharev, "Pulsed MHD Power System SAKHALIN-The World Largest Solid Propellant Fueled MHD Generator of 500MWe Electric Power Output.," *In Proceedings of 13th International Conference on MHD Power Generation and High Temperature Technologies,* vol. 2, pp. 387-398, October 1999.

[18] B. L. Liu, J. T. Lineberry, Y. C. L. Wu, H. J. Schmidt, Y. Changqi and J. Zixiang, "Three-Dimensional Analysis of the IEE MARK II MHD Generator.," *9th International Conference on Magnetohydro-dynamic Electric Power Generation,* vol. 1, pp. 313-322, 1986.

[19] T. Takahashi, T. Fujino and M. Ishikawa, "Comparison of Generator Performance of Small-Scale MHD Generators with Different Electrode Dispositions and Load Connection Systems," *Journal of International Council on Electrical Engineering,* vol. 4, no. 3, pp. 192-198, 2014.

[20] T. Murakami, Y. Okuno and H. Yamasaki, "Achievement of the highest performance of a CCMHD generator: an isentropic efficiency of 63% and an enthalpy extraction ratio of 31%.," *IEEE transactions on plasma science,* vol. 32, no. 5, pp. 1886-1892, 2004.

[21] P. Marco, B. Betti and F. Nasuti, "Coupled analysis of hot-gas and coolant flows in LOX/methane thrust chambers.," *4th European Conference on Aerospace Sciences, St. Petersburg, Russia, EUCASS ,* vol. 134, 2011.

[22] C. H. Marchi, F. Laroca, A. F. Carvalho da Silva and J. N. Hinckel, "Numerical Solutions of Flows in Rocket Engines with Regenerative Cooling," *Numerical Heat Transfer, Part A,* vol. 45, pp. 699-717, 2004.

[23] S.-K. Kim, M. Joh, H. S. Choi and T. S. Park, "Effective Modeling of Conjugate Heat Transfer and Hydraulics for the Regenerative Cooling Design of Kerosene Rocket Engines," *Numerical Heat Transfer, Part A: Applications,* pp. 863-883, 2014.

[24] S.-K. Kim, M. Joh, H. S. Choi and T. S. Park, "Multidisciplinary simulation of a regeneratively cooled thrust chamber of liquid rocket engine: Turbuent combustion and nozzle flow," *International Journal of Heat and Mass Transfer,* vol. 70, pp. 1066-1077, 2014.

[25] H. W. Zhang, Y. L. He and W. Q. Tao, "Numerical study of film and regenerative cooling in a thrust chamber at high pressure," *Numerical Heat Transfer, Part A,* vol. 52, pp. 991-1007, 2007.

[26] M. Pizzarelli, B. Betti and F. Nasuti, "Coupled analysis of hot-gas and coolant flows in LOX/methane thrust chambers," in *4th European Conference for Aerospace Sciences*, 2011.

[27] M. Pizzarelli, F. Nasuti and M. Onofri, "Coupled Numerical Simulation of Wall Heat Conduction and Coolant Flow in Liquid Rocket Engines," in *47th AIAA/ASME/SAE/ASEE Joint Propulsion Conference & Exhibit*, San Diego, California, 2011.

[28] T.-S. Wang and V. Luong, "Hot-Gas-Side and Coolant-Side Heat Transfer in Liquid Rocket Engine Combustors," *Journal of Thermophysics and Heat Transfer,* 1994.

[29] Y. Feng, H. Huang, T. Li, D. Zhang and Z. Wang, "Flow Field and Heat Transfer Analysis of Local Structure for Regenerative Cooling Panel," *Journal of Thermal Science,* vol. 21, 2012.

[30] O. Vidana, M. Chaidez, B. Lovich, J. Aboud, M. Hernandez, L. Cabrera and N. Love, "O. Vidana, M. Chaidez, B. Lovich, J. Aboud, M. Hernandez, Component and System Modeling of a Direct Power Extraction System," *54th AIAA Aerospace Sciences Meeting,* p. 243, 2016.

[31] I. Ansys, ANSYS Fluent Theory Guide, Ansys,Inc, 2016.

[32] I. Ansys, ANSYS Meshing User's Guide, Ansys, Inc., 2013.

APPENDIX

DPE COMBUSTOR ASSEMBLY

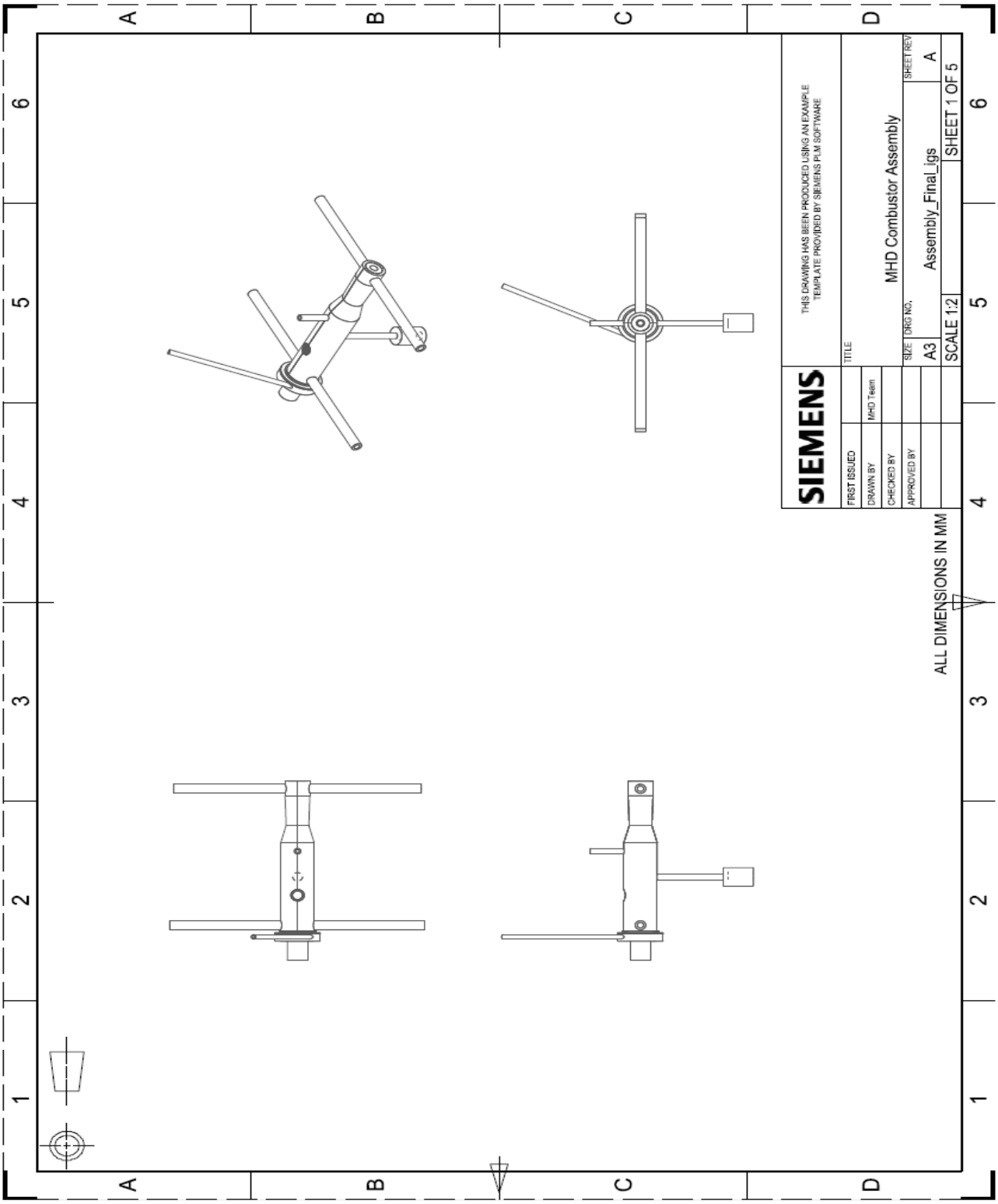

DPE COMBUSTOR EXPLODED VIEW

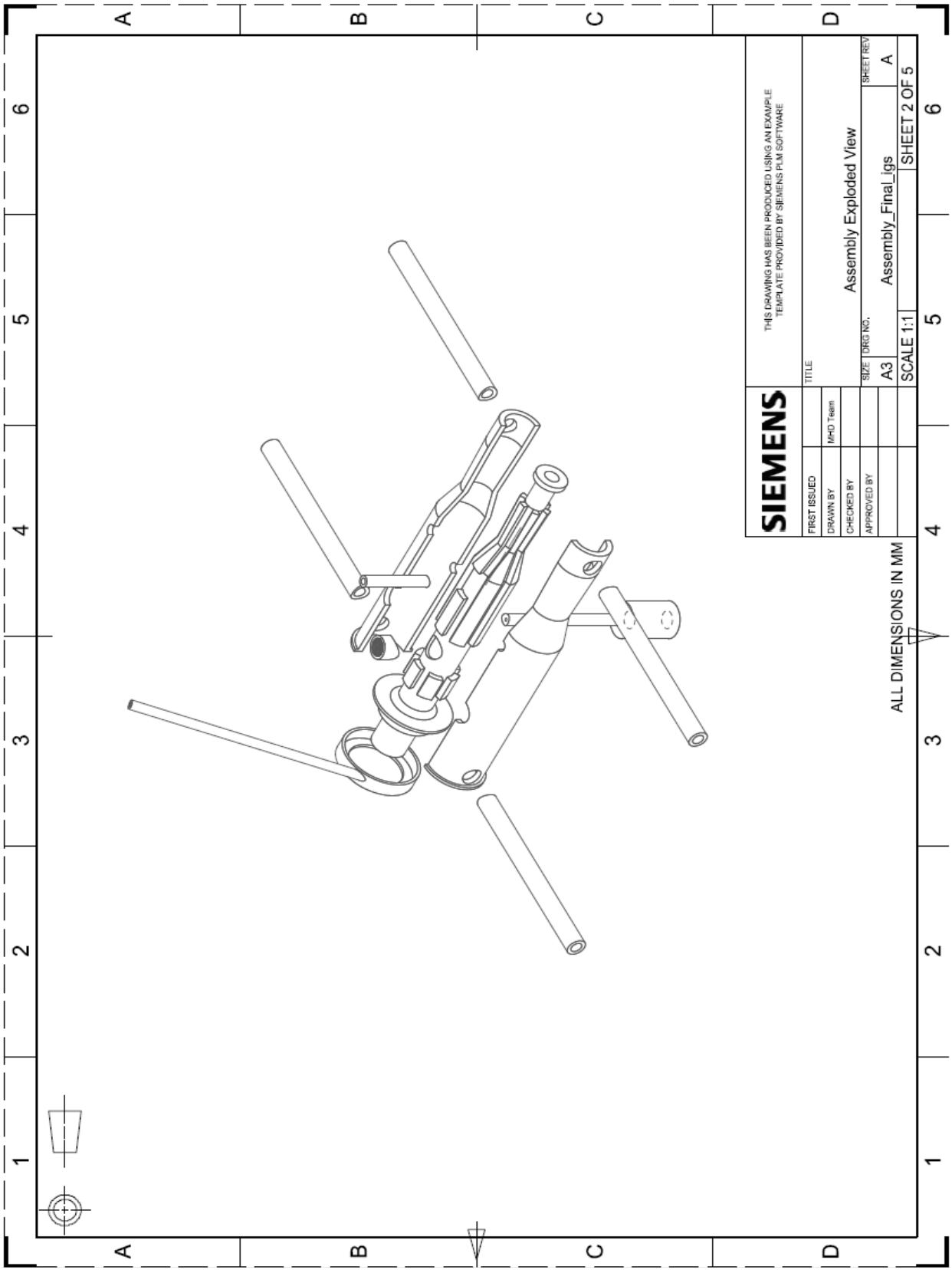

Matlab Code for experimental

IMPORT DATA TO WORKSPACE

IIMPORTANT: copy "importfile.m" to the directory which contains the data Data = IMPORTFILE(FILENAME, STARTROW, ENDROW) Reads data from rows STARTROW through ENDROW of text file FILENAME.
1st column is Time 2nd column is Fuel flow rate 3rd column is Oxygen flow rate 4th column is Water flow rate 5th column is Water inlet Pressure 6th column is Water outlet Pressure 7th column is Oxygen Pressure 8th column is Fuel Pressure 9th column is Combustion chamber Pressure 10th column is Oxy inlet temperature [correct the name] 11th column is water outlet temperature 12th column is water inlet temperature 13th column is Fuel inlet temperature [correct the name] 14th column is Combustion Chamber temperature

```
clc
clear
fpath = input('Enter the path where to save your Figure:    ','s');
filename =input('Insert file track as a string:       ','s');
data =  importfile(filename,25,60000);
s = size(data);
```

EXTRACT DATA COLUMNS

```
time = data(:,1);   %Time
FF1 = data(:,2);    % Fule Flow Rate
OF1 = data(:,3);    % Oxi Flow Rate
WP1 = data(:,5);    % Water inlet Pressure
WP2 = data(:,6);    % Water outlet Pressure
OP1 = data(:,7);    % Oxi Pressure
FP1 = data(:,8);    % Fuel pressure
CP1 = data(:,9);    % Combustion Chamber Pressure
WT2 = data(:,11);    % water outlet temperature
CT1 = data(:,13);    % Combustion Chamber temperature
    WT2(isnan(WT2)) = 0 ;
        for i= 1:s(1)
            if eq(WT2(i),0)
                 WT2(i) = WT2(i-1);
            end
        end
WT1 = data(:,12);    % water inlet temperature
    WT1(isnan(WT1)) = 0 ;
        for i= 1:s(1)
            if eq(WT1(i),0)
                WT1(i) = WT1(i-1);
            end
        end

FT1 = data(:,13);    % Fuel inlet temperature [correct the name]
    FT1(isnan(FT1)) = 0 ;
        for i= 1:s(1)
            if eq(FT1(i),0)
```

```
                FT1(i) = FT1(i-1);
            end
        end
OT1 = data(:,10);    % Oxi inlet temperature [correct the name]
    OT1(isnan(OT1)) = 0 ;
        for i= 1:s(1)
            if eq(OT1(i),0)
                OT1(i) = OT1(i-1);
            end
        end
```

SMOOTHING DATA

```
FF1s = smooth(FF1,50);
OF1s = smooth(OF1,50);
WP1s = smooth(WP1,50);
WP2s = smooth(WP2,50);
OP1s = smooth(OP1,50);
FP1s = smooth(FP1,50);
CP1s = smooth(CP1,50);
WT2s = smooth(WT2,50);
WT1s = smooth(WT1,50);
FT1s = smooth(FT1,50);
OT1s = smooth(OT1,50);
CT1s = smooth(CT1,50);
```

PLOTTING

```
%%%Plot the Pressure Vs. Time

createfigure_pressure(time, [OP1s FP1s CP1s])

saveas(gcf, fullfile(fpath, 'Pressure'), 'jpeg')


%%%Plot The Flowrate Vs. Time

createfigure_flowrate(time, [OF1s FF1s])
saveas(gca, fullfile(fpath, 'FlowRate'), 'jpeg')

%%%Plot The Temperature Vs. Time

createfigure_temperature(time,[CT1s WT2s WT1s])
saveas(gca, fullfile(fpath, 'Temperature'), 'jpeg')

%%%calculate plot the delta Temperature drop

dt = WT2 - WT1;
dts = smooth(dt,1000);
createfigure_dt(time, dts)
saveas(gca, fullfile(fpath, 'Temperature drop'), 'jpeg')
```

```
%%%Plot The OF Vs. Time

rhoo = 1.41;
rhof = 0.668;
mo= rhoo*OF1s;
mf= rhof*FF1s;
of = mo./mf;
ofs = smooth(of,50);
createfigure_OF(time, ofs)
saveas(gca, fullfile(fpath, 'OF'), 'jpeg')

%%%HEAT Flux

% mw = input(' Enter the water flow rate in GPM:       ')
    mw = (4.65*0.00399*996)/60;
%      v = (mw*0.0000631)/((0.00225)^2*6);
    v =mw/(996*0.00003167);
    twavrg = (WT2+WT1)/2;
    twavrgs = smooth(twavrg,1000);
    rhow =  -0.0025.*twavrgs.^2 - 0.1948.*twavrgs + 1003.2;
    k = -9E-06*twavrgs.^2 + 0.0021.*twavrgs + 0.5604;
    muw = 1E-07.*twavrgs.^2 - 2E-05.*twavrgs + 0.0014;
    mu = 1E-07.*CT1s.^2 - 2E-05.*CT1s + 0.0014;
    cp = (1E-05.*twavrg.^2 - 0.0009.*twavrg + 4.1943)*1000;
    deltat = CT1s - twavrgs;
       mw = (4.7*0.00399.*rhow)/60;
    D = 0.00225;
        h = ((k/D).*0.023).*(((D*v.*rhow)./(mu)).^0.8).*(((mu.*cp)./k)).^0.4.*(mu./muw).^.167;
    q = (h.*deltat)/1000000;
    qs = smooth(q,1000);
createfigure_HeatFlux (time, qs)
saveas(gca, fullfile(fpath, 'Heat Flux'), 'jpeg')

%%%Heat out from the coolant

% Q = m. cp. delta t
 qc = mw.*cp.*(WT2s-WT1s)/1000;
 mf = FF1s.*rhof/(1000*60);
 hhv = 55528000;
 Fi = hhv.*mf;
  qcs = smooth(qc,1000);
 HR = (qcs./Fi)*1000;
 HRs = smooth(HR,50);

createfigure_heatremoved(time, qcs)
saveas(gca, fullfile(fpath, 'Heat Removed'), 'jpeg')
```

VITA

Jad G. Aboud first joined UTEP in Fall 2012 as an undergraduate student in Mechanical Engineering and graduated from the program with a GPA of 3.79. Upon graduation in Spring 2015, he was awarded the Superior Achievement Award for his exceptional performance throughout his undergraduate studies. However, his desire for more knowledge and education led him to join the graduate program in the College of Engineering to aspire further studies in aerospace and combustion. From an undergraduate to a graduate Research Assistant at the Center for Space Exploration Technology Research Lab under the supervision of Dr. Norman Love Jr., Jad's primary research interest led him to team up with other researchers to design, model, and test a supersonic, liquid-cooled combustor intended to be used in a direct power extraction system. His work during the project resulted in three publications; one as the primary author "2-D Computational Model of A Coaxial Swirl Fuel Injector," and two of which as a co-author "Review of MHD Power Generation Systems", "Computational Modeling of Isentropic Flow Through a Conical Nozzle"- awarded best paper by the AIAA Terrestrial Committee at the 2016 SciTech Conference in San Diego, California. Once graduating with his master's degree in Mechanical Engineering, Jad will pursue his Ph.D. to achieve further success in this field.

Contact Information: Jaboud@miners.utep.edu

This thesis was typed by Jad G. Aboud